A synthetic planar cell polarity system reveals localized feedback on Fat4-Ds1 complexes

Olga Loza[1*], Idse Heemskerk[2*], Nadav Gordon-Bar[1], Liat Amir-Zilberstein[1], Yunmin Jung[1] and David Sprinzak[1]

[1] Department of Biochemistry and Molecular Biology, Wise Faculty of Life Science, Tel Aviv University, Tel Aviv, Israel

[2] Department of Biosciences, Rice University, Houston, Texas, USA

[*] Equally contributing authors

Abstract

The atypical cadherins Fat and Dachsous (Ds) have been found to underlie planar cell polarity (PCP) in many tissues. Theoretical models suggest that polarity can arise from localized feedbacks on Fat-Ds complexes at the cell boundary. However, there is currently no direct evidence for the existence or mechanism of such feedbacks. To directly test the localized feedback model, we developed a synthetic biology platform based on mammalian cells expressing the human Fat4 and Ds1. We show that Fat4-Ds1 complexes accumulate on cell boundaries in a threshold-like manner and exhibit dramatically slower dynamics than unbound Fat4 and Ds1. This suggests a localized feedback mechanism based on enhanced stability of Fat4-Ds1 complexes. We also show that co-expression of Fat4 and Ds1 in the same cells is sufficient to induce polarization of Fat4-Ds1 complexes. Together, these results provide direct evidence that localized feedbacks on Fat4-Ds1 complexes can give rise to PCP.

Introduction

Planar cell polarity (PCP) defines the coordinated polarization of cells in the plane of tissue[1-5] and underlies the organization and geometry required for the proper function of many developing organs. PCP is usually manifested by orientation of external structures, such as trichomes and sensory hair cells in *Drosophila* [5,6], and hair structures in the inner ear and skin of vertebrates[7-9].

At the molecular level, PCP is defined by asymmetric distribution of transmembrane protein complexes which belong to two families - the Frizzled/Van-Gogh pathway (termed the "core" pathway) and the Fat/Dachsous (Ft/Ds) pathway. Both were discovered in *Drosophila* but are conserved in higher vertebrates[5,10,11].

The main players in the Ft/Ds pathway in *Drosophila* are the large atypical cadherins Ft, Ds and the Golgi protein kinase Four-jointed (Fj). Ft and Ds take part in heterophilic interactions resulting in trans-hetero-complexes on the boundary between cells. Unlike classical cadherins, there is no evidence of homophilic complexes of either Ft or Ds forming across cells [12,13].

The mammalian homologues of Ft and Ds include Fat1-4 and Ds1-2. However, Fat4 and Ds1 have the highest homology to *Drosophila* Ft and Ds, are the most widely expressed, and have the strongest knockout phenotypes[14]. Fat4 and Ds1 null mice show complex morphological abnormalities in the inner ear, kidney, brain, bone,

lymph node, and more. [9,15]. In humans, mutations in Fat4 and Ds1 were recently linked to various cancers and abnormal brain development[16,17]. Unlike in *Drosophila*, polarized distributions of Fat4 and Ds1 in vertebrates have not been observed yet, probably due to lack of good reagents for staining these proteins *in-vivo*.

It remains poorly understood how polarized distribution of Fat and Ds is established, and how it is coordinated between neighboring cells. Models for the emergence of polarity can be classified according to whether or not they include feedbacks. Models without feedback propose that observed gradients of Ds and Fj are sufficient to explain the asymmetric distribution of Fat-Ds complexes[18-23]. However, these models cannot explain how relatively small differences in Ds and Fj expression between neighboring cells can lead to strongly polarized membrane distributions.

This problem is solved by models that include localized feedback mechanisms, where we define "localized" to mean a feedback at the level of protein complexes within the cell boundary, to distinguish it from transcriptional feedback or tissue scale feedbacks. Such models have been previously proposed to explain polarity in the core pathway, where the localized feedbacks are mediated by the cytoplasmic proteins Prickle and Dishevelled[24-26]. However, no such feedbacks were identified for the Fat-Ds pathway.

In principle, two localized feedback mechanisms can be distinguished: (1) a self-enhancing feedback that promotes the formation of additional Ft-Ds complexes in the same direction of existing Ft-Ds complexes, and (2) a mutual inhibition feedback between complexes in opposite direction (Figure 1A). Mathematical modeling predicts that models with both feedbacks can amplify small differences in expression and create strongly polarized cell boundaries [27,28]. Intuitively, a model with a self-enhancing feedback alone would lead to roughly equal numbers of opposing complexes, whereas a model with mutual inhibition feedback alone would remove pairs of opposing complexes and leave only the small excess of the dominant complex type. The combination of both feedbacks together leads to strong accumulation of complexes in one direction. Somewhat less intuitive is the prediction of these models that polarity can emerge spontaneously once threshold levels of Ft and Ds are reached, even in the absence of external gradients[27,28]. We note that models for PCP based on the core pathway are equivalent to mutual inhibition feedback described above and do not require self-enhancing feedback.

To test whether localized feedbacks are required for establishing Fat4-Ds1 mediated planar cell polarity, it is necessary to directly verify their existence and the prediction of spontaneous polarization in the presence of threshold expression levels. In this work, we develop an experimental synthetic biology platform to study the interactions of Fat4 and Ds1 in live mammalian cells. By analyzing co-cultures of cells expressing Fat4 fused to Citrine and cells expressing Ds1 fused to mCherry, we show that Fat4-Ds1 complex formation exhibits a threshold response to the levels of Fat4 and Ds1, supporting a localized self-enhancing feedback mechanism. We further show that Fat4-Ds1 complexes at the cell boundary form extremely stable clusters, suggesting that complex stabilization through clustering may serve as a mechanism for localized feedback. Finally, we show that cells expressing both Fat4 and Ds1 exhibit strong localized polarization, supporting the existence of mutual inhibition between opposing complexes. We find that the direction of polarization depends on the relative levels of Fat4 and Ds1 across the boundary between cells.

Results

Development of an experimental system for quantitative characterization of the mammalian Fat4/Dachsous1 interactions

To study the interactions between Fat4 and Ds1 at the boundary between cells we cloned the full length human Fat4 with a c-terminal fusion of Citrine (Fat4-Citrine) and the human Ds1 with a c-terminal fusion to mCherry (Ds1-mCherry) (Figure 1B). We generated HEK293 stable cell lines expressing Fat4-Citrine under a constitutive CMV promoter (HEK-Fat4-Citrine) and Ds1-mCherry under a doxycycline inducible promoter (HEK-Ds1-mCherry). Western blotting confirmed that these fusion proteins were expressed and showed the expected molecular bands at ~500kDa for Fat4-citrine and~320kDa for Ds1-mCherry (Figure1- figure supplement 1A).

To study the interactions between Fat4-Citrine and Ds1-mCherry we performed co-culture experiments of HEK-Fat4-Citrine and HEK-Ds1-mCherry (Figure 1C-F). Consistent with the existing evidence for exclusively heterotypic interactions, these co-culture experiments revealed strong accumulation of Fat4-Citrine and Ds1-mCherry at heterotypic junctions (yellow arrows in Figure 1D-F), while no accumulation was observed in homotypic junctions (white arrows in Figure 1D) or in

monoculture experiment of either cell line (Figure 1- figure supplement 1B-C). Similar accumulation was observed in co-culture experiments of MCF7 cells expressing the same fusion constructs (Figure 1- figure supplement 1D).

Surprisingly, we also found that Ds1-mCherry *trans*-endocytoses into the Fat4-citrine cells as evident from numerous vesicles containing both Ds1-mCherry and Fat4-Citrine (white triangles in insets Figure 1D-F, see also yellow vesicles in Figures 3 and 4, and in movie S1). No trans-endocytosis of Fat4-Citrine into the Ds1-mCherry cells is observed. This observation is the first evidence for the presence of transendocytosis in Ft-Ds pathway.

Accumulation of Fat4-Ds1 complexes requires threshold levels of Ds1 and Fat4

Having confirmed the expected qualitative behavior of our synthetic PCP system, we set out to determine how the accumulation of Fat4-Ds1 complexes depends on the expression levels of Fat4-citrine and Ds1-mCherry. To separately test the effect of self-enhancing and mutual inhibition feedbacks, we first considered co-culture of Fat4-citrine and Ds1-mCherry expressing cells, where mutual inhibition feedback is not present as opposing complexes cannot be formed. We began by analyzing the accumulation of Fat4-citrine and Ds1-mCherry at the population level in snapshots of co-culture experiments with Ds1-mCherry induction periods varying from 0 to 20 hours (Figure 2A-B). We used automated image analysis to segment the cells and boundaries, and measure the Fat4-citrine and Ds1-mCherry fluorescence levels in each cell and each boundary (Figure 2C). By analyzing tens of thousands of junctions per condition we obtained detailed statistical information about the effect of increased Ds1-mCherry expression on Fat4-Ds1 accumulation.

A self-enhancing positive feedback model is expected to exhibit a non-linear dependence of the accumulation of complexes on the total Ds1-mCherry level in the cell. To test this prediction we measured the fraction of accumulating boundaries and the average Ds1-mCherry expression in images (Figure 2 - figure supplement 1A-B). We find that relation between these quantities is best fitted with a Hill function with a Hill coefficient of $n = 2.2 \pm 0.3$, whose value $n > 1$ is consistent with a localized positive feedback model (Figure 2D). A somewhat stronger non-linear response ($n =$

4.5 ± 1.3) was observed in a second experiment where Ds1 levels where induced to lower levels (Figure 2 – supplement figure 2A-C).

Having analyzed the population averages we next wanted to test if accumulation on a cell boundary is associated with locally higher expression levels of Fat4-citrine and Ds1-mCherry. For each Ds1 induction time, we compared the distributions of Fat4 and Ds1 expression in cells that have strong accumulation on their boundary ('accumulating boundaries', Figure 2E-F, dashed lines) and cells that do not ('non-accumulating boundaries', Figure 2E-F, solid lines). We found that cells with accumulating boundaries generally express higher levels of either Fat4 or Ds1 (Figure 2E-F, solid vs. dashed lines, 20h time point). We note that even with long induction times not all Fat4-Ds1 boundaries exhibit accumulation.

To test if accumulation on boundaries simultaneously requires high levels of Fat4-citrine and high levels of Ds1-mCherry, we plotted for each induction time, the two-dimensional distribution of the levels of Fat4-citrine and Ds1-mCherry in the cells flanking all boundaries (Figure 2G-H, Figure 2- figure supplement 1C, Figure 2 – figure supplement 2C) (In Figure 2H, each dot represents one boundary and the axes values indicate the levels of Fat4-Citrine and Ds1-mCherry in the cells flanking that boundary). We observed a clear separation between 'accumulating boundaries' (yellow dots in Figure 2H) and 'non-accumulating boundaries' (boundaries without accumulation) (purple dots in Figure 2H) indicating that accumulation occurs when both Fat4-citrine and Ds1-mCherry are expressed above a certain threshold level. Note that, while the fraction of boundaries exhibiting accumulation increased with induction time (Figure 2- figure supplement 1C, Figure 2- figure supplement 2D), the separation between the two populations (i.e the threshold levels) remained almost the same (dashed lines Figure 2H). Such a behavior is expected from a localized feedback model exhibiting bistability.

Live imaging reveals threshold response of Fat4-Ds1 accumulation dynamics at the single cell level

Analysis of the snapshots demonstrated a threshold dependence of Fat4-Ds1 complexes on Fat4-citrine and Ds1-mCherry levels, however it does not show the time scale of accumulation on individual boundaries. Moreover, the non-linear response in population level measurements may be smeared by averaging over many

cells. To test whether a threshold response is also observed at the single cell level, and how abrupt the onset of accumulation, we performed live cell imaging of single Fat4-Ds1 boundaries during Ds1-mCherry induction.

To look at the accumulation of single boundaries over time we performed experiments using the two-cell assay – a micropatterning based method previously used by us and others to look at single pairs of cells over extended time periods[29] (Figure 3A). We also tracked single Fat4- and Ds1-expressing cell pairs in a free co-culture assay (Figure 3 – supplement 1A). We then quantified the total Fat4 and Ds1 levels as well as the accumulation of Fat4-Ds1 complexes on the cell boundary over time after induction of Ds1-mCherry expression (Figure 3B and movie S1, Figure 3- figure supplement 1A-C). While the total Fat4 levels do not change, the total Ds1 levels increase slowly above background level, and become observable about 100min after addition of doxycycline (see Figure 3 - supplement figure 2A-C). This delay in observed fluorescence is probably due to maturation time of mCherry, as mRNA levels increase linearly upon induction (Figure 3 – supplement figure 2D). We note that most Ds1-mCherry is localized on the cell membrane, even in the absence of Fat4 expressing cells (Figure 3 – supplement figure 2A-C), and that the measured total and membrane Ds1 levels are proportional, justifying the use of total Ds1-mCherry as a measure of the relevant Ds1 level in the cell.

The accumulation of Fat4-citrine and Ds1-mCherry proteins on the boundary between cells shows a sharp increase shortly after Ds1 levels starts increasing (Figure 3C, Figure 3- figure supplement 1A-C). Furthermore, Ds1-mCherry on the boundary continues to increase faster than the total Ds1 (i.e. in a non-linear fashion) for several hours after accumulation starts (Figure 3 – supplement figure 1F), consistent with a threshold response. Taken together, the population snapshot experiments (Figure 2) and the single cell time lapse movies (Figure 3) strongly support a non-linear threshold response of Fat4-Ds1 complexes to the levels of Fat4 and Ds1.

Fat4 and Ds1 accumulation are proportional, consistent with stoichiometric binding

Although Fat4 and Ds1 accumulate on the boundary between cells, it is not clear whether this accumulation reflects the formation of heterotypic complexes or the independent recruitment of unbound Fat4 and Ds1 on both sides of the boundary. To

distinguish between these two scenarios we analyzed the relative accumulation of both proteins in single cell movies. It is expected that feedback on complex formation would maintain a fixed stoichiometric ratio between Fat4 and Ds1, while independent accumulation (or independent feedback) of unbound Fat4 and Ds1 would not. Analysis of the three movies described above (Figure 3C and Figure 3- figure supplement 1B-C) showed that Fat4 and Ds1 fluorescence at the accumulating boundary are proportional as the boundary is formed (spanning over two orders of magnitude in fluorescence) (Figure 3D and Figure 3- figure supplement 1D-E). Similar results were obtained by analyzing snapshots from 31 boundaries showing, again a high degree of correlation (ρ=0.989) over two orders of magnitudes in fluorescence (Figure 3E). This linear relation between the accumulation on both sides of the boundary indicate the formation of Fat4-Ds1 complexes with a fixed stoichiometric ratio.

Fat4 and Ds1 form extremely stable complexes on the boundary

We next wanted to understand the mechanism of localized self-enhancing feedback. It has been previously shown that cadherins can interact cooperatively across the cell boundary to promote cell adhesion [30,31]. We therefore hypothesized that stabilization of Fat4-Ds1 complexes, possibly through clustering, can be an underlying mechanism for the self-enhancing feedback. Although strictly, such a mechanism would predict increased complex stability at increased complex concentration, one would at the very least expect a large difference in stability between bound Fat4-Ds1 complexes and unbound Fat4 and Ds1. Consistent with this idea, increased stability of Ft-Ds complexes was recently observed in localized puncta on cell boundaries in *Drosophila* [21].

To test the stability of Fat4-Ds1 complexes, we performed fluorescent recovery after photobleaching (FRAP) experiments on boundaries exhibiting accumulation (Figure 4A-B, movie S2). Experiments were performed by bleaching the Fat4-citrine fluorescence (green in Figure 4A), without affecting the Ds1-mCherry fluorescence (red in Figure 4A), allowing automated tracking of the recovery dynamics of Fat4-citrine on the boundary. Analysis of the recovery profile over time showed very slow recovery time (>25 minutes) on the accumulating boundary (see boundary on

kymograph in Figure 4B), reflecting the extremely low turnover and membrane dynamics of Fat4-Ds1 complexes.

We then examined whether the slow recovery of complexes is a reflection of the slow dynamics of unbound Fat4 and Ds1 or of the increased stability of the complex. To analyze the membrane dynamics of Fat4 and Ds1 we used FRAP combined with total internal reflection fluorescence microscopy (FRAP-TIRF) [32]. We performed these experiments on monocultures of Fat4-citrine (Figure 4C-D, movie S3) and Ds1-mCherry (Figure 4- figure supplement 1A-B). Both Fat4-citrine and Ds1-mCherry exhibited very fast recovery compared to the Fat4-Ds1 complexes, of the order of a few seconds (Figure 4B and D and Figure 4- figure supplement 1B). Quantitative analysis of FRAP movies allowed estimating the effective diffusion coefficients and membrane-cytoplasm exchange rates of Fat4-Ds1 complexes as well as unbound Fat4 and Ds1 (see methods). We found that the mean diffusion coefficient of Fat4-Ds1 complexes is more than two orders of magnitude smaller than that of unbound Fat4 and Ds1 (Figure 4E). Similarly, the mean exchange rate of Fat4-Ds1 complexes are significantly smaller than those of the unbound Fat4 and Ds1 (Figure 4F). Hence, complexes formed on the boundary between cells show extremely high stability compared to unbound Fat4 and Ds1.

To test if the observed slow dynamics is specific to Fat4-Ds1 complexes we also analyzed the dynamics of both unbound and bound *N*-cadherin-GFP (*N*-cad-GFP) (Figure 4- figure supplement 1C-F) using the same experimental approach. Similar to the results with Fat4 and Ds1, we found that accumulation of *N*-cad-GFP complexes on the cell boundary exhibited significantly slower dynamics than unbound *N*-cad-GFP (Figure 4E-F and Figure 4- figure supplement 1C-F). This result is consistent with cooperative binding and enhanced stabilization of complexes at the boundary as previously observed for E-cadherin [33]. Overall, these results support a model where stabilization of Fat4-Ds1 complexes via clustering serves as a mechanism for localized self-enhancing feedback.

Finally, we also note that unbound Fat4 exhibited significantly faster membrane diffusion than unbound Ds1 (Figure 4E) despite having a significantly higher molecular weight (500KDa vs 320KDa). This suggests that either Ds1 diffusion is somehow inhibited compared to Fat4, or that the surface dynamics of Fat4 are enhanced through active transport processes.

Boundary accumulation of Fat4 and Ds1 exhibits a 100-200nm gap

Previous work on *Drosophila* Ft and Ds showed that Ft-Ds complexes form puncta along the cell boundaries[21,34]. To examine the spatial structure of Fat4-Ds1 complexes in our system we performed high resolution imaging of these boundaries. Unlike the *Drosophila* case, but consistent with a previous report[15] in mammalian cells, we mostly observe continuous accumulation along the boundary. However, surprisingly, we observed a spatial gap between the peak in red fluorescence (Ds1-mCherry) and the peak in green fluorescence (Fat4-citrine) along the boundary (Figure 5A-C). We refer to this gap as the 'rainbow' feature (Figure 5B). Rainbows were apparent in most boundaries exhibiting accumulation in both HEK293 and MCF7 cells (Figure 5- figure supplement 1A-H). This shift is not due to chromatic aberration, as images of cells taken with fluorescent beads show clear rainbows even after the chromatic aberration was corrected (Figure 5- figure supplement 1I-N). Furthermore, we observed that different boundaries in the same picture and even the same cell (when both Fat4 and Ds1 are co-expressed) can exhibit oppositely directed rainbows (see Figure 6B). A similar shift was observed in images taken in super resolution STED microscopy (Figure 5- figure supplement 1E-H).

Quantitative analysis of 61 boundaries revealed a relatively tight distribution of gaps with mean and standard deviation of 116±63nm (Figure 5D). Such a gap between the c-termini of Fat4 and Ds1 (where the fluorophores are fused to) is consistent with the length of Fat4 and Ds1 bound to each other in an extended linear form. Given that the length of a cadherin ectodomain is 4.5nm[35], we estimate the extended form of the complex should be at least 150nm ($34\times4.5nm = 153nm$ assuming full overlap between Fat4 and Ds1) (Figure 1B).

Cells expressing both Fat4 and Ds1 exhibit localized polarization

Polarity *in vivo* is established in cells expressing both Fat and Ds, with Ds and Fat activity or expression controlled by a morphogen gradient[21,36,37]. The localized feedback model, however, predicts that polarization can emerge spontaneously; i.e. without external gradients[27]. To test if our synthetic cell culture system can polarize without tissue scale gradients we generated stable HEK293 cells that expressed both Fat4-citrine and inducible Ds1-mCherry (Figure 6A). Upon induction of Ds1-

mCherry expression we observed clear accumulation of Fat4-citrine and Ds1-mCherry on the boundary between cells (Figure 6B), similar to the accumulation observed in co-culture of Fat4-citrine and Ds1-mCherry cells (Figure 1D-F).

Analysis of high resolution images (Figure 6C) revealed rainbows similar to the ones observed in co-culture experiments (Figure 5). The observed rainbows show that even in cells expressing both Fat4-citrine and Ds1-mCherry, there is a strong bias in the direction of complex formation on any given cell-cell boundary. Furthermore, we generally do not see domains of opposite polarity within single boundaries suggesting that complexes on cell boundaries align in a coordinated manner. This observation is consistent with mutual inhibition feedback between complexes and suggests that direct interaction between opposing complexes is sufficient for generating polarity.

The direction of polarity depends on differences in Fat4 and Ds1 expression

Interestingly, we see that the direction of polarity, i.e., the direction from green to red in the rainbow (black arrow in Figure 6D), can differ between boundaries of the same cell (see, for example, boundaries 2, 3, and 4, in Figure 6B-D). This behavior is different from the long range polarization of Ft-Ds observed in Drosophila wing and larvae[19,34,37,38], but is reminiscent of polarity reversal within the same cell recently observed in *Drosophila* larvae denticles[39].

We hypothesized that the difference between the localized polarity observed in the cell culture system and the coordinated polarity observed *in vivo* may be due to the variability in expression of Fat4 and Ds1 in our system and that this variability results in expression differences across the boundaries that locally bias the polarity. To check this hypothesis, we measured the differences in cytoplasmic levels of Fat4 and Ds1 across each boundary. We defined the direction of expression gradients as the directions going from low to high expression level of Fat4 and Ds1 (marked by red and green triangles in Figure 6D). We then checked whether the direction of polarization, determined by the rainbow feature (red-green polarity bar in Figure 6D), is aligned with the direction of expression gradients of Fat4 and Ds1 across the boundary. We found that when the expression gradients of Fat4 and Ds1 are opposed (such as in boundaries 1,2, and 4 in Figure 6D) the polarity aligns with both the Ds1 and Fat4 gradients. Namely, that boundary accumulation of Ds1 occurs on the cell with higher Ds1 expression, and conversely, boundary accumulation of Fat4 occurs

on the cell with higher Fat4 expression. However, in situations where both expression gradients are aligned (such as in boundary 3 in Figure 6D) we found that the direction of polarity can align either with the Fat4 gradient or with the Ds1 gradient. An analysis of 107 boundaries (Figure 6E), indeed showed that if Fat4 and Ds1 expression gradients are opposed, then the polarity almost always aligned with the direction of both gradients (bottom pie chart in Figure 6E). On the other hand, when Ds1 and Fat4 expression gradients were aligned (top pie chart in Figure 6E) we got almost equal number of boundaries aligned with Ds1 gradient (33 out of 68) and boundaries aligned with the Fat4 gradient (27 out 68). This result is consistent with a situation where the polarity is either controlled by the Ds1 expression gradient or controlled by the Fat4 expression gradient, depending which of the two is dominant.

To check whether the final direction of polarity reflects the expression gradients that existed prior to the formation of polarized accumulation, we performed live imaging of boundary formation using confocal Airyscan technology. The movie of boundary accumulation (Figure 6 – supplement figure 1) confirms that the rainbow feature emerges in the direction of the Ds1 expression gradient (no significant Fat4 expression gradient is observed in this movie). Overall, these observations support a picture where localized polarization of Fat4-Ds1 complexes in cell culture is biased by local gradients generated by cell-to-cell variability.

Discussion

In this work, we have adopted a synthetic biology approach to planar cell polarity and reconstituted Fat4-Ds1 PCP in a cell culture system to elucidate the basic mechanisms underlying polarity establishment. Reducing the *in vivo* system to its core allows dissecting Fat4-Ds1 interactions in a controlled and quantitative manner, beyond what is possible *in vivo*. The *in vivo* relevance of the *in vitro* findings can then subsequently be verified in a targeted manner.

Two classes of models have been proposed to explain the emergence of asymmetric distribution of PCP proteins on cell boundaries: (i) gradient models, claiming that the asymmetric distribution of PCP proteins reflects the external gradients controlling the level and/or activity of PCP proteins[21,37], and (ii) localized feedback models, where small initial biases in complex polarity are amplified by a combination of self-enhancing feedback between like complexes and mutual inhibition feedback between

opposing complexes[24-28] (Figure 1A). Our results strongly support the existence of such localized feedbacks in the Fat4-Ds1 system and suggest a potential mechanism driving these feedbacks.

By analyzing co-culture of cells expressing only Fat4 or Ds1 we can analyze the existence and properties of self-enhancing localized feedbacks in the absence of mutual inhibition. Large scale snapshot analysis (Figure 2) and live cell imaging of single pairs (Figure 3) show that accumulation of complexes at the boundary exhibits a threshold response to increasing levels of Ds1 - a hallmark of positive feedback. This is the first direct observation of a positive feedback loop in a PCP system. Evidence for the second class of localized feedback, the mutual inhibition between opposing complexes, is provided by our finding that strong polarization is consistently found in cells expressing both Fat4 and Ds1, even in the absence of a strong expression gradient in either of the proteins (Figure 6).

What could be the mechanism behind the localized feedbacks on Fat4-Ds1 complexes? The strong polarization and inferred presence of both feedbacks in a minimal synthetic system make it plausible that no other proteins specific to this pathway are involved in the feedback, and favor simple mechanisms that rely on direct interaction of the heterotypic complexes. Both positive and negative feedback can act either at the level of production or degradation. For example, for the positive feedback case, complexes can either catalyze production of like complexes, or prevent degradation of like complexes. Using quantitative FRAP analysis we show that unlike unbound Fat4 and Ds1, Fat4-Ds1 complexes are extremely stable, and do not recover or diffuse even after several minutes. This observation suggest that the positive feedback could at least in part rely on enhanced stability of complexes, possibly through cluster formation. Such enhanced stability of clusters was shown to occur with other cadherin such as E-cadherin[31,33]. Furthermore, FRAP analysis of Drosophila Ft/Ds in wing disk junctions also showed enhanced stability on boundary puncta compared to other boundary regions[21].

Enhanced stability mechanism may not be the only mechanism contributing to localized feedbacks. For example, clusters could not only stabilize complexes but also catalyze their formation by acting as a “diffusion trap”, as has also been suggested for E-Cadherin[40]. Moreover, work in Drosophila has implicated directional trafficking[41] and feedbacks through cytoplasmic PCP components[24] as other potential mechanisms for localized feedbacks.

One potential difficulty with the extreme stability of Fat4-Ds1 complexes is that it may be hard for the cells to change their initial polarity, for example to respond to cell divisions or morphogenetic processes. Interestingly, the observed trans-endocytosis of Ds1 into the Fat4 cell (Figure 1D-F) may serve as a way to quickly remodel boundaries in spite of their slow turnover by removing large fragments of boundaries with otherwise stable Fat4-Ds1 complexes.

Our finding that polarity of Fat4-Ds1 accumulation at the cell boundary can be observed with optical microscopy through the gap between Fat4 and Ds1 fluorescence (Figure 5) is surprising. The expected lengths of the extracellular domains of Fat4 and Ds1 in an extended form are 153nm and 121nm, respectively (Fat4 and Ds1 have 34 and 27 cadherin repeats, respectively). Hence, the observed gaps are consistent with the length of Fat4 and Ds1 in an extended conformation. A recent study, however, suggested that Fat4 and Ds1 fold into a compact structure to fit into intercellular gaps[42]. It is unclear whether these seemingly contradictory observations are due to different methodologies or different cellular contexts. Hence, further experiments are required to determine the structural basis of the observed gaps in our experiments.

We used our synthetic system to show that cells expressing both Fat4 and Ds1 exhibit polarized distribution of these proteins on cell-cell boundaries. Hence, our *in vitro* setup shows that expression of Fat4 and Ds1 is sufficient to generate polarized boundaries. Unlike *in vivo* tissues where the direction of polarity is coordinated over extended regions, the direction of polarity of each boundary in our *in vitro* assay seem to be independent of the polarity of nearby boundaries. It is possible that this difference is due to the relatively large cell-to-cell variability in the expression of Fat4 and Ds1 in cell culture. This variability can lead to local effective gradients of Fat4 and Ds1 biasing the direction of polarity in each boundary. This situation is reminiscent of the disordered organization of denticles in *Drosophila* larvae which was attributed to variability in Ds expression between different rows[39,43].

Analysis of the direction of Fat4 and Ds1 gradients across each boundary indeed shows that for the unambiguous situation of opposing Fat4 and Ds1 gradients, the polarity (determined independently by the ‘rainbow’ feature) aligns with the local gradients. For the case where gradients are incompatible (i.e. pointing in the same direction), the polarity may be determined by either the Fat4 or the Ds1 gradients, depending which one is more dominant (e.g. which gradient is stronger).

Our results and conclusions are not limited to the understanding of Fat-Ds signaling but provide a general framework for how complex local interactions between membrane proteins can induce tissue level organization. It remains to be seen whether similar mechanisms occur also in other systems.

Acknowledgments

We would like to thank Helen McNeil for advice and support. This work was supported by a grant from the Israeli Science Foundation (grant no. 545/14).

Methods

Cloning of Fat4 and Ds1

Human Fat4 and Ds1 cDNA sequence were amplified from the mRNA extracted from MCF7 (ATCC HTB-22, RRID:CVCL_0031) cell line. Several fragments of each gene were amplified and then combined using either restriction enzymes or Gibson assembly[44]. The Citrine and mCherry were fused to the *C*-terminal end of the full length Fat4 and Ds1, respectively. Fat4 fusion construct was placed under a CMV constitutive expression promoter, while Ds1 fusion construct was placed under a doxycycline inducible promoter (pcDNA5/TO, T-REx system, Thermofisher).

Cell culture and transfection

HEK293 (ATCC CRL1753, RRID:CVCL_0063) cells were grown in adherent cultures in Dulbecco's Modified Eagle's Medium (DMEM) supplemented with 10% FBS. MCF7 cells were grown in Eagle's Minimum Essential Medium supplemented with 10% FBS and 0.01 mg/ml human recombinant insulin (Biological Industries). All cells were cultured in a humidified atmosphere of 5% CO_2 at 37^{o}C. Stable and transient transfections were performed using *Trans*IT®-LT1 reagent (Mirus Bio) according to the manufacturer's instructions. For Fat4 and Ds1 constructs 1 µg of the plasmid was taken, for the other plasmids the mixture of the desired plasmid (200ng) with an empty vector (800ng).

Both HEK293 and MCF7 cells are in the list of commonly misidentified cell lines maintained by the International Cell Line Authentication Committee. These two cell lines serve as a cellular platform for the testing the interactions between Fat4 and Ds1 in the current work. These cells were chosen since they are standard epithelial cell lines which are often used in *in-vitro* experiments. Furthermore, HEK293 cells do not endogenously express Fat4 and Ds1 and hence provide an ideal platform to study these proteins.

STR profiling confirmed the authentication of the MCF7 cell line but showed significant genetic modifications in the HEK-Fat4-Citrine and HEK-Ds1-mCherry cells, which is consistent with the known genomic instability of the HEK293 cell line. We note that both cell lines are clonal as they were grown from single cell colonies. The specific properties of these cells are not a contributing factor in our synthetic biology platform, nor do we compare between cell lines. For transparency purposes, we will make these cell lines available through a public repository (e.g. ATCC). All

our cell lines tested negative for mycoplasma. Tests were performed using the EZ-PCR mycoplasma kit (Biological Industries).

Stable cell line establishment

For the generation of stable cell lines, transiently transfected cells were passaged 24 h post-transfection in growth medium containing the appropriate selection antibiotics for 10 days (Zeocin (InvivoGen, USA) 100µg/ml for Fat4-citrine constructs, Blasticidin 5µg/ml and Hygromicin (AG Scientific,USA) 50µg/ml for MCF7 and 100µg/ml for HEK293 cells (AG Scientific,USA) for Ds1-mcherry constructs).

Single cell colonies were generated by limiting dilution in a 96-well plate (2 cells/ml). After a period of two weeks, the plates were screened for positive clones, which were transferred to a new plate for further growing.

HEK293 cell line expressing both Fat4-citrine and inducible Ds1-mCherry was generated by consecutive transfection and selection processes for both constructs.

SDS page and Western blot

Protein samples were prepared by trypsinization of HEK293 cells ($1x10^6$ cells). The cells were washed by PBS buffer and then lysed by adding 2x Laemmli sample buffer supplemented with 2M urea and boiled for 10 minutes. Samples of cell extracts were separated by SDS-PAGE (GeBARunner, DNR Bio-Imaging Systems) under reducing conditions using 4-12% gradient polyacrylamide gels (DNR Bio-Imaging Systems) according to manufacturer's instructions.

The samples were then electrophoretically transferred for 16 hours in 4^oC using wet transfer standard protocol to the nitrocellulose membranes. Blots were blocked for 1 hour in PBST (PBS buffer and 0.1 % Tween) containing 5% skim milk, followed overnight incubation at 4°C with anti-GFP (Cell signaling, RRID:AB_390710) and anti-mCherry (Clontech, RRID:AB_10013483) primary antibodies . Blots were washed three times and incubated for 1 hour at room temperature with the secondary antibody (HRP-conjugated goat anti-rabbit IgG, Jacksonimmuno, RRID:AB_2307391). Immunoreactive bands were visualized by the enhanced chemiluminescence method (ECL) (Biological Industries) according to standard procedures.

qPCR Analysis

HEK-Ds1-mCherry cells were grown for 24hrs. Doxycycline (DOX) was added for 0, 0.5, 1 and 2 hrs. RNA was isolated with TRIzol® reagent (Life Technologies). 1 µg of RNA was reversed transcribed (SuperScript® III, Termo Fisher Scientific). mRNA expression was evaluated with the TaqMan® Gene Expression Assay (Applied Biosystems) using the FastStart Universal Probe Master (Roche). Relative expression of the mRNAs was normalized to GAPDH. Real-time PCR was performed in triplicate.

Primers sequence:

For mCherry: Forward: AGGACGGCGAGTTCATCT, Reverse: CCCATFGTC TTCTTCTGCATTA

For GAPDH: Forward: GCTGGCATTGCCCTCAAC, Reverse: CATGAGGTCCAC CACCCTG

Cell preparation for snapshot analysis and free co-culture experiments, FRAP and FRAP-TIRF experiments

A co-culture/monoculture of Fat4-citrine and Ds1-mCherry expressing cells (1.6×10^4 cell/ml) was seeded onto 24-well glass bottom plates (Cellvis, USA) or 35mm plates (SPL lifesciences, Korea) 12 hours prior the imaging.

For snapshot analysis assay the 24-well plates were covered with 50ug/ml of Concanavalin A (Sigma Aldrich) to improve cell adherence. Cells were grown for 12 hours and then for induction of Ds1-mCherry, 100ng/ml doxycycline (Sigma-Aldrich) was added to the growth medium for various periods of time. After that the cells were washed with PBS and fixed for 15 minutes at room temperature with 2% paraformaldehyde in PBS. To visualize nuclei, the cells were stained with Hoechst Stain solution (Sigma Aldrich) for 5 minutes.

For FRAP on boundaries and FRAP-TIRF, the cells were seeded on 24-well plates and 35mm plates, respectively. Directly prior the imaging the media was replaced with low fluorescence imaging media (αMEM without Phenol red, ribonucleosides, deoxyribonucleosides, folic acid, biotin and vitamin B12 (Biological Industries, Israel)). For induction of Ds1-mCherry expression, 100ng/ml doxycycline (Sigma-Aldrich) was added to the growth medium 12 hours prior to imaging.

Micropatterns

Micropatterning was performed as previously described [45], In brief, A PDMS mold with raised bowtie patterns was attached to a glass surface of the 6-well glass bottom plates (MatTek, USA) after being treated with a UV/Ozone cleaning device (UVOCS, USA). Liquid agarose (0.6% in 2:3 EtOH:ddH_2O) was wicked into the gap between the mold and the glass and an inverted pattern of agarose was formed upon removal of the PDMS mold. Bovine Fibronectin (50 µg/ml, Biological Industries) was adsorbed on the exposed regions of the glass by incubating it for 1hr at room temperature. The square size of the bowties used was 20x20µm which yielded the highest probability of a single cell to attach in each half of the bowtie. The mix of HEK293-Fat4-citrine and HEK293-Ds1 cells was diluted to 1.6×10^4 cell/ml and seeded onto the patterned plate. Directly prior imaging the media was replaced with a previously mentioned low fluorescence imaging media. For induction of Ds1-mCherry, 100ng/ml doxycycline (Sigma-Aldrich) was added to the growth medium to induce expression.

Microscopy details

Imaging of fixed cells for snapshot analysis

Cells were imaged using Nikon TI-E inverted microscope (Nikon, Japan) equipped CFI Plan Apo 20X objective NA=0.7 (Nikon, Japan); and an ANDOR sCMOS camera (Andor, Belfast, Northern Ireland). The equipment was controlled by Micro-Manager 1.4 software (UCSF). For each field of view 10 planes with 1µm apart in the z direction were taken.

FRAP on the accumulating boundaries

FRAP experiments on the accumulating boundaries were performed using Andor revolution spinning disk confocal microscope supplied with FRAPPA device (Andor, Belfast, Northern Ireland). Photobleaching was performed with 70% power of the 445nm laser for a total bleach time of 75ms (3 repeats of 25ms).

FRAP-TIRF experiments

Cells were imaged in FRAP-TIRF iMIC system (Till photonics) equipped with an oil-immersion Plan-Apochromatic 100x objective NA=1.45 (Olympus, Tokyo, Japan) and an ANDOR iXon DU 888D EMCCD camera (Andor, Belfast, Northern Ireland). FRAP protocol is similar to the one described previously in Khait et al (Khait).

Live cell imaging of Fat4-Ds1 movies

Cells were imaged using Andor revolution spinning disk confocal microscope (Andor, Belfast, Northern Ireland). The imaging setup consisted of an Olympus inverted microscope with an oil-immersion Plan-Apochromatic 60x objective NA=1.42

(Olympus, Tokyo, Japan); and an ANDOR iXon Ultra EMCCD camera (Andor, Belfast, Northern Ireland). For Fat4-citrine and Ds1-mCherry co-culture movies (Figure 3), 90 images were taken every 10 minutes with exposure of 500ms. For each time point 8-12 z planes every 1µm were taken.

Movies of Ds1-mCherry activation (Figure 3 – figure supplement 2) were performed using a Zeiss LSM880 confocal microscope. Images were taken every 5 minutes. For each time point 7 z-planes every 1µm were taken.

The movie of cells expressing both Fat4-citrine and Ds1-mCherry (Figure 6 – figure supplement 1) was performed using Zeiss LSM880 confocal microscope equipped with Airyscan detection unit. Image were taken every 5 minutes.

High resolution confocal imaging and super resolution imaging

High resolution images were acquired either with a Leica TCS SP5 (Leica Microsystems, Wetzlar, Germany) of with Leice TCS SP8 (Leica Microsystems, Wetzlar, Germany). The SP5 setup included HC PL APO 63x/1.40 Oil STED objective.

For the super resolution images we used Leica TCS SP8 equipped with a STED module and an HC PL APO 100x/1.40 Oil STED objective and white laser. For STED images, the white light laser was set on excitation wavelength of 510nm or 586nm with an emission window of 520-581nm or 605-647nm, using the 592nm or 660nm depletion laser to narrow the PSF of the signal thus improving resolution. Deconvolution of the acquired images was performed with the Huygens Pro software on default settings.

Data analysis

Snapshot analysis

Prior to analysis, z stacks of all the images were converted to 'average intensity projection' images. Snapshots of Fat4-Ds1 co-culture were segmented using Ilastik[46], an open source software for image classification and segmentation (http://ilastik.org/) and custom written Matlab code. One classifier was trained on the Fat4-citrine and Ds1-mCherry signal to distinguish regions of Fat4 expressing cells, Ds1 expressing cells and background. A second classifier was trained on the co-localization signal of Fat4-citrine and Ds1-mCherry complexes to identify accumulating boundaries with the 'intensity feature' turned off to prevent inadvertently thresholding to identify boundaries and thereby creating a bias. A final classifier identified nuclei based on the

Hoechst signal. Cells were then segmented by using the nuclei for a seeded watershed of the Fat4-Ds1 regions. For cells where the classifier failed to identify the cell type, raw Fat and Ds intensity was used to assign the type. Accumulating boundaries were assigned to cell interfaces based on their presence in cells on a dual lattice generated by watershedding the interfaces. Distributions in Fig 2 were generated from mean intensities in each cell shifted to have the dimmest cells have value 10, a cutoff value used for the log scale binning. Bins were spaced evenly on the log scale so the graphs show P(log I). In 2D histograms a fixed lookup table for the probabilties was used for different time points and intensity distributions for interfaces with and without accumulation were normalized by the sum of the two distributions (the total number of cells). All analysis code can be found at https://github.com/idse/FatDs/ . Intensity values used to generate the distributions in figure 2 and figure 2 - supplement figure 2 can be found in the alldata.xlsx file.

Fat4-citrine and Ds1-mCherry accumulation movies

Prior to analysis, z stacks of all the images were converted to 'average intensity projection' images. Fat4-citrine and Ds1-mCherry accumulation movies were analyzed using semi-automatic custom written Matlab code. Cells were first segmented be mapping Fat4-citrine cells (green) and Ds1-mCherry cells (red), then the total fluorescence in these areas was measured. The overlap between the red and green areas was mapped as accumulating boundary. Since Ds1-mCherry fluorescence levels are low at short induction time; the segmentation by the code was not complete. In these cases we manually corrected the segmentation using DIC images for proper cell recognition.

FRAP analysis of Fat4-Ds1 accumulating boundary

Boundaries were segmented and tracked using the open active contour method (snake) implemented in the ImageJ plugin JFilament [47] on the unbleached Ds1-mCherry signal. Using custom written Matlab code the Fat4-citrine signal along the snake was obtained as the maximal intensity projection normal to the snake over a 9 pixel wide strip. Given the drift and growth / shrinkage of the snakes over times, the signal along the snake at different times had to be registered by maximizing the spatial cross-correlation to produce the space time profile. For Fat4-Ds1 boundaries we bleached half the boundary. We then fit an error function to the profile at each time, adapting [48], i.e. at each time we fit:

$$f(x) = U_0\left(1 - A\frac{1 + \mathrm{erf}\left(\frac{x-x0}{L}\right)}{2}\right)$$

The diffusion constant was then obtained by fitting the linear relation with the squared width of the error function, which follows $L^2 = L_0^2 + 4Dt$, while the exchange rate is the time scale obtained from fitting an exponential decay to the dynamics of A. The reason for doing things this way rather than fitting a spacetime profile directly is an increased robustness against registration errors, growth and shrinkage of the snakes and overall brightness changes cause by boundary drift in z.

Image analysis of FRAP-TIRF experiments.

All data processing was performed using custom written Matlab code, as described in Khait et al. [32]. We used a semi-automatic analysis code for FRAP data extraction and fitting procedure. In brief, we defined for each movie a region of interest around the bleached area. The fluorescence profile as a function of time was extracted, corrected for background level and photobleaching and averaged along the axis parallel to the bleached stripe resulting in 1D fluorescence profile for each time point. Fitting to the recovery profiles for extracting Diffusion coefficients and exchange were done according to Khait et al.[32]

Rainbow analysis and gradient measurements

As in the boundary FRAP analysis, boundaries for rainbow analysis were segmented using Jfilament. Using custom written Matlab code intensities were interpolated on equaly spaced points along the boundary and along lines normal to the boundary to create a straightened intensity image. For each position on the boundary the intensity profile normal to the boundary was then fitted by a Gaussian. The relative position of the Fat and Ds peaks defines the direction of the polarity in Fig 6, while the distribution of the distance between the peaks for each position along each boundary is shown in Fig 5D. To determine gradients for Fig 6, cytoplasmic intensities were determined by taking the summed intensity projection of 5 slices centered round the plane of the rainbow, and then measuring the total intensity in a box away from the boundary, excluding the nucleus using the DAPI image and excluding vesicles using an intensity threshold.

Figure captions

Figure 1: Fat4-Citrine and Ds1-mCherry accumulate on heterotypic boundaries. **(A)** Schematic of the localized feedback hypothesis. **(B)** Schematic illustration of the stable cell lines and fusion constructs of Fat4-citrine and inducible Ds1-mCherry. **(C)** Schematic illustration of the cell-cell boundaries formed in a co-culture assay of Fat4-citrine (green) and Ds1-mCherry (red) cells. Yellow boundary represents accumulation at heterotypic boundaries. *Yellow vesicles represent trans*-endocytosis of Ds1-mCherry into Fat4-citrine expressing cells. **(D-F)** A co-culture of HEK-Fat4-citrine cells (green) and HEK-Ds1-mCherry cells (red). Strong accumulation is observed in heterotypic boundaries (yellow arrows). No accumulation is observed in homotypic boundaries (White arrows). Zoom in on the accumulation area (white box in D) demonstrates that Ds1-mCherry trans-endocytoses (white triangles) into Fat4-citrine expressing cell (but not vice-versa). Nuclei are stained with Hoechst (blue). Scale bar - 20 µm. Supplementary figure (Figure 1- figure supplement 1) shows Western blot analysis, monoculture images from the two cell lines and boundary accumulation in MCF7 cell line.

Figure 1- figure supplement 1: Fat4-citrine and Ds1-mCherry accumulate on heterotypic boundaries, but not on homotypic boundaries (A) Fat4-Citrine and Ds-mCherry are expressed stable cell lines based on Hek293 cells. Cell lysates from stable cell lines of Fat4-citrine and Ds1-mCherry were analyzed by Western blotting using anti-GFP and anti-mCherry antibodies. The high molecular bands are observed at the expected ~500kDa for Fat4-citrine and~320kDa for Ds1-mCherry. **(B-C)** An image of monocultures of cells expressing Ds1-mCherry (B) and Fat4-citrine (C). No accumulation is observed at homotypic boundaries in monocultures. Scale bar -10µm. **(D)** A co-culture of MCF7-Fat4-citrine cells (green) and MCF7-Ds1-mCherry cells (red). Heterotypic boundary exhibits accumulation (yellow arrow). Scale bar - 10µm.

Figure2: Accumulation on the boundary between cells requires threshold levels of Fat4-citrine and Ds1-mCherry. **(A-C)** The analysis pipeline for Fat4-Ds1 boundary accumulation. **(A)** Snapshots of HEK-Fat4-citrine (green) and HEK-Ds1-mCherry (red) co culture, at different Ds1 induction times. Nuclei are stained with Hoechst (blue). Higher Ds1-mCherry (red) levels are observed for longer induction times. Scale bar -100 µm. **(B)** Zoom in on the area marked with rectangle in (A) shows both accumulating (yellow arrows) and non accumulating (white arrows)

boundaries. Scale bar – 20 μm. **(C)** Segmentation of the 20h induction time point (right image in (B)). Left image shows overlay of the cell segmentation while right image shows the segmentation label for cell type and boundary accumulation (green – Fat4, red – Ds1, yellow – accumulating boundary, blue – nuclei). **(D)** Plot showing the increase in the fraction of accumulating boundaries with Ds1-mCherry levels. Different colors represent different doxycycline induction times. Hill function fit (solid line) gives a Hill coefficient of $n = 2.2 \pm 0.3$**,** showing nonlinear increase. The error on *n* represent 95% confidence interval of the fit. **(E-F)** Probability distribution functions (pdf) of the total (cytoplasm+boundary) Fat4-citrine levels (E) and Ds1-mCherry levels (F) in cells exhibiting accumulation on heterotypic boundaries (dashed lines) and in cells not exhibiting accumulation on heterotypic boundaries (solid lines). Pdf's shown are for the case of 20h doxycycline induction time. **(G)** Schematic of the defined 'accumulating' and 'non accumulating' boundaries. **(H)** Two dimensional distributions of the expression levels of Fat4-citrine and Ds1-mCherry in cells flanking each boundary after 0, 5 and 20 hours induction with doxycycline. Each point in the histogram corresponds to one Fat4-Ds1 boundary (see schematic in G), and the 'x' and 'y' values correspond to the levels of Ds1-mCherry and Fat-citrine flanking that boundary, respectively. Both axes are in logarithmic scale. The clear separation between 'accumulating boundaries' (yellow) and 'non-accumulating boundaries' (purple) indicates the threshold concentrations of Ds1 and Fat4 (dashed lines) above which a boundary is formed. Supplementary figure 1 (Figure 2- figure supplement 1) shows the average Ds1-mCherry expression, fraction of accumulation, and the distributions of accumulating and non-accumulating boundaries in all induction times. Supplementary figure 2 (Figure 2- figure supplement 2) shows the results of a duplicate experiment but with slightly different Ds1 induction rates.

Figure 2- figure supplement 1: Accumulation on the boundary requires high levels of both Fat4 and Ds1. **(A-B)** The fraction of cells with accumulation at their boundaries **(A)** and the average Ds1-mCherry level in each image **(B)** increase as a function of induction time. Each dot represent the value obtained from one image. **(C)** Two dimensional distributions of the expression levels of Fat4-citrine and Ds1-mCherry in cells flanking each boundary. The plots demonstrate the distributions at different induction times as described in Figure2. Each point in the histogram corresponds to one Fat4-Ds1 boundary, where yellow points correspond to

'accumulating boundaries' and purple points correspond to 'non-accumulating boundaries'. Both axes are in a logarithmic scale.

Figure 2- figure supplement 2: Accumulation on the boundary requires high levels of both Fat4 and Ds1. Analysis of a second experiment similar to the one shown in Figure 2 and Figure 2 – supplement Figure 1. In this experiment Ds1 induction levels were lower. **(A-B)** The fraction of cells with accumulation at their boundaries (A) and the average Ds1-mCherry level in each image (B) increase as a function of induction time. Each dot represent the value obtained from one image. **(C)** Plot showing the increase in the fraction of accumulating boundaries with Ds1-mCherry levels. Different colors represent different doxycycline induction times. Hill function fit (solid line) gives a Hill coefficient of n=4.5±1.3, showing nonlinear increase. The error on n represent 95% confidence interval of the fit. **(D)** Two dimensional distributions of the expression levels of Fat4-citrine and Ds1-mCherry in cells flanking each boundary. The plots demonstrate the distributions at different induction times as described in Figure2. Each point in the histogram corresponds to one Fat4-Ds1 boundary, where yellow points correspond to 'accumulating boundaries' and purple points correspond to 'non-accumulating boundaries'. Both axes are in a logarithmic scale.

Figure 3: Live imaging of Fat4-Ds1 accumulation dynamics reveals threshold response to Ds1 levels at the single cell (A) Schematic of the two-cell assay. In this assay two cells are restricted to a bowtie-shaped microwell allowing imaging of accumulation dynamics over time. **(B)** A filmstrip showing a movie in the two-cell assay with HEK-Fat4-Citrine cell (green) co-cultured with a HEK-Ds1-mCherry cell (red) (see Supplementary movie S1). Imaging started after the addition of the 100 ng/ml doxycycline. Each image in the filmstrip is a sum of 8 z-slices encompassing the total width of the cells. As Ds1 levels increases, both proteins co-localize and accumulate at the cell boundary (yellow arrow). Scale bar - 10μm. **(C)** Quantitative analysis of accumulation dynamics. The levels of total cellular Fat4-Citrine (green solid line), total cellular Ds1-mCherry (red solid line), boundary Ds1-mCherry (red dashed line), and boundary Fat4-citrine (green dashed line) are plotted as a function of post-induction time. The fluorescence of both proteins exhibit a threshold response

(black dashed line. **(D-E)** Mean boundary levels of Fat4-citrine and Ds1-mcherry are proportional to each other. Analysis of the single cell movie (D) and snapshots (E) shows that Fat4 and Ds1 fluorescence at the accumulating boundary are proportional to each other. ρ and n, correspond to the Pearson correlation coefficient and the number of frames, respectively. Supplementary figure 1 (Figure 3- figure supplement 1) shows accumulation dynamics of free co-culture experiments and the non-linear accumulation of all movies shown here. Supplementary figure 2 (Figure 3- figure supplement 2) shows the distribution and dynamics of membrane Ds1 vs. total Ds1 in the cell.

Figure 3- figure supplement 1: Live imaging of Fat4-Ds1 accumulation dynamics in free co-culture reveals threshold response to Ds1 levels (A) A filmstrip showing a movie from a free co-culture (i.e. not in a two cell assay) with Hek-Fat4-Citrine cell (green) co-cultured with a Hek-Ds1-mCherry cell (red). Imaging started two-hours after the addition of 100ng/ml doxycycline. Each image in the filmstrip is a sum of 13 z-stacks encompassing the total width of the cells. As Ds1 levels increase, both proteins co-localize and accumulate at the cell boundary (yellow arrow). Scale bar - 10μm. **(B-C)** Quantitative analysis of accumulation dynamics in two free co-culture movies. Here (B) is the analysis of the movie shown in (A) and (C) is the analysis of an additional free co-culture movie (not shown). The levels of total cellular Fat4-Citrine (green solid line), total cellular Ds1-mCherry (red solid line), boundary Ds1-mCherry (red dashed line), and boundary Fat4-citrine (green dashed line) are plotted as a function of post-induction time. Scale bar - 10 μm. **(D-E)** Analysis of the single cell movies in (B-C) shows that Fat4 and Ds1 fluorescence at the accumulating boundary are proportional to each other. **(F)** A log-log plot of Ds1 levels on the accumulating boundaries as a function of total Ds1 levels in the cell. The three plots correspond to the data shown in Fig. 3C (orange), Fig. 3 – supplement figure 1B (blue), and Fig. 3 – supplement figure 1C (blue). Slopes higher than 1 (black dashed line) indicate non-linear accumulation of Fat4-Ds1 complexes as a function of Ds1 in the cell.

Figure 3- figure supplement 2: The membrane fraction of Ds1 mCherry is large and proportional to the total Ds1-mCherry in the cell. (A) Snapshot from a confocal time-lapse movie tracking dynamics and localization Ds1-mCherry levels in

Hek-Ds1-mCherry cells. Ds1-mCherry was imaged at 7 z-planes. 1μm apart, every 5 minutes, starting 32 minutes after doxycycline induction. Ds1-mCherry is localized both to the cell membrane (z=0μm plane) and to intracellular vesicles (see intracellular spots inside the cells at z=3μm plane). Scale bar - 10μm. **(B)** The mean Ds1-mCherry level at the z=0μm plane, corresponding to the membrane fluorescence, as a function of time. Fluorescence of Ds1-mCherry levels starts increasing about 100 minutes after doxycycline induction. The data shown is an average of four movies and the error bar represent the standard error of the mean. This delay is probably due to finite maturation time of Ds1-mCherry. **(C)** The mean membrane Ds1-mCherry level (measures at z=0μm) is proportional to the mean total Ds1 mCherry levels (mean over all z-planes). **(D)** Fold change in Ds1 mRNA levels measured by qPCR show that the expression increases linearly in the first 2 hours showing that the delay in fluorescence levels observed in (B) is not due to delay in expression. Ds1 mRNA levels in each sample were normalized to GAPDH mRNA. Fold change is measure with respect to the mRNA levels with no doxycycline induction (t=0). The values shown are the average of three independent repeats and the error bars represent the standard error of the mean.

Figure 4. Bound Fat4-Ds1 complexes on the boundary are more stable than unbound Fat4 and Ds1. (A) A filmstrip showing a fluorescence recovery after photobleaching (FRAP) experiment on a boundary exhibiting accumulation (yellow) of Fat4-citrine (green) and Ds1-mCherry (red). (see Supplementary movie S2) **(B)** A kymograph showing the fluorescence recovery profile along the boundary outlined in blue in (A). The fluorescence level (gray scale) is shown as a function of the position along the boundary (x-axis), and the time after photobleaching (y-axis). **(C)** A filmstrip from FRAP-TIRF experiment on a cell that express Fat4-citrine (see Supplementary movie S3). Arrow indicates the bleached area. **(D)** A kymograph showing the fluorescence recovery profile in the bleached area in (C). Almost full recovery of the bleached area is obtained after 20 sec. Scale bars - 5 μm. **(E-F)** Distributions of Diffusion coefficients (E) and exchange rates (F) obtained from analysis of FRAP experiments as those shown in (A-D). * and *** correspond to p-value<0.05 and p-value<0.001, respectively, as estimated by t-test. The number of experiments for each sample are: unbound Fat4 n=29, unbound Ds1 n=36, unbound *N*-cadherin n=21, Fat4-Ds1 complex n=10, *N*-cadherin complex n=11. Error bars correspond to SEM. Supplementary figure (Figure 4- figure supplement 1) shows the analysis for unbound Ds1-mcherry, unbound *N*-cadherin-GFP, and the bound *N*-cadherin complex.

Figure 4- figure supplement 1: Unbound Ds1-mCherry and *N*-cadherin-GFP exhibit fast membrane dynamics (A-D) Filmstrips and analysis of FRAP-TIRF experiments on Hek293 cells express Ds1-mCherry (A-B) and *N*-cadherin-GFP (C-D)**.** Scale bar - 5 μm. For the *N*-cadherin experiments, Ds1-mCherry cells were transiently transfected with *N*-cadherin-GFP constructs. Frapped region is indicated arrows. **(B,D)** Kymographs showing the fluorescence recovery profile in (A) and (C), respectively. The fluorescence level (gray scale) is shown as a function of the position along the bleached area (y-axis), and the time after photobleaching (x-axis). **(E)** A filmstrip showing a FRAP experiment on a boundary exhibiting accumulation of *N*-cadherin-GFP. The experiment was performed in a similar way to the FRAP experiments with Fat4-citrine and Ds1-mCherry accumulating boundaries (Figure 4A). **(F)** A kymograph showing the recovery profile in (E).

Figure 5. Fat4-citrine and Ds1-mCherry fluorescence at the boundary between cells are shifted by 100-200nm. (A) A high resolution image of a boundary exhibiting a 'rainbow' feature (composed of three stripes green, yellow and red; white arrow) indicating a shift between red and green fluorescence. Scale bar - 5 μm. **(B)** An illustration of the observed 'rainbow' feature. **(C)** A straightened version of the boundary shown in A (top). Fluorescence profiles (bottom) of Fat4-citrine (green) and Ds1-mCherry (red) along lines perpendicular to the boundary. Mean gap size for this boundary is as indicated **(D)** Probability distribution function of the distance between the peaks in the fluorescence profiles. Mean gap width for 61 boundaries as indicated. Supplementary figure (Figure 5- figure supplement 1) shows control experiments in MCF7 cells, super resolution STED images, and rainbows after correction of chromatic aberrations.

Figure 5- figure supplement 1: The rainbow feature is observed in other cell types and with super resolution microscopy. (A-C) A rainbow feature observed in a confocal image of a co-culture of Fat4-citrine and Ds1-mCherry in MCF7 cells. Scale bar - 10 μm**. (D)** A zoom in on the boundary in (C). Scale bar - 2μm. **(E-G)** A super-resolution image of the rainbow feature in a stimulated emission depletion (STED) microscope (Here, the co-culture is the same as Figure 5A). Scale bar - 2μm**. (H)** A zoom in on the boundary in (G). Scale bar - 0.5 μm. **(I-N)** High resolution confocal

890 images of a rainbow next to a 100nm tetraspeck bead (marked by an arrow). (I) A raw
891 image of the boundary without any correction. Scale bar - 2.5μm. (J) A zoom in on
892 the bead in (I). (K) A zoom in on the boundary in (I). Scale bar - 0.5μm. (L) The
893 image in (I) after correction of chromatic aberration. The correction of chromatic
894 aberration was performed by applying global conformal transformation over the
895 whole image (not shown) that minimizes the distances between the centers of the
896 beads in the two channels. While the correction eliminates the shift between the two
897 channels on the bead (M), the rainbow feature in the boundary is maintained (L,N).
898
899 **Figure 6. Fat4-citrine and Ds1-mCherry polarize in cells expressing both**
900 **proteins. (A)** Schematic illustration of the stable cell lines expressing both Fat4-
901 citrine and inducible Ds1-mCherry in the same cell. **(B)** An image of HEK293 cells
902 expressing both Fat4-citrine and Ds1-mCherry. A rainbow feature (composed of three
903 stripes green, yellow and red) is evident at the boundary between the cells. Scale bar -
904 10 μm. **(C)** Zoom in on the boundaries in (B) marked by the numbers 1-4. Each
905 boundary is presented next to its schematic illustration. Scale bar - 1 μm **(D)** An
906 illustration of all the cells and boundaries shown in (B). The red-green barbells
907 indicate the direction of polarity as determined by analysis of the rainbow. In this
908 notation, the red and green circles marks the 'red side' and the 'green side' of the
909 rainbow, respectively (see schematic of the notation on the right panel). The red and
910 green triangles represent the directions of the cytoplasmic Ds1 and Fat4 gradients
911 between the two cells flanking the boundary, respectively (cytoplasmic levels where
912 measured in the area adjacent to the boundary – see methods). **(E)** Pie charts showing
913 how the direction of polarization (red-green barbell) aligns with either the Fat4
914 expression gradient (green triangle), or the Ds1 expression gradient (red triangle), or
915 both, in the 107 analyzed boundaries. In the boundaries where the Fat4 and Ds1
916 gradients are opposed (bottom pie chart) the polarity almost always (36 out of 39)
917 aligns in a direction compatible with both gradients. In the boundaries where the Fat4
918 and Ds1 gradients are aligned (top chart), the polarity cannot be compatible with both
919 gradients. In these cases, it aligns with the Fat4 gradient in about half of the
920 boundaries (27 out of 68), and to the Ds1 gradient in the other half (33 out of 68). NP
921 – Non-polarized boundaries (no clear rainbow observed).
922

Figure 6 – figure supplement 1. Polarization aligns with the expression gradient that existed prior to boundary accumulation. (A) A filmstrip from a movie of HEK293 cells expressing both Fat4-citrine and Ds1-mCherry showing the emergence of accumulation in a boundary (white rectangle). Bottom strips – straightened versions of the boundaries in the filmstrip. Scale bar - 5µm **(B)** A schematic showing the direction of the expression gradient of Ds1 in (A) at t=200min. The level of Fat4 is almost equal between the two cells flanking the boundary. **(C)** Fluorescence profiles of Fat4-citrine (green) and Ds1-mCherry (red) along lines perpendicular to the boundary at t=200min. **(D)** A histogram showing the distribution of the gap widths observed in the fluorescence profiles in (C). Mean gap size for this boundary is as indicated.

Movie S1: A timelapse movie showing the dynamics of Fat4-Ds1 accumulation in a single cell pair. Movie used to generate filmstrip in Figure 3B.

Movie S2: A timelapse FRAP movie showing the dynamics of bound Fat4 in Fat4-Ds1 complex on the accumulating boundary. Movie used to generate filmstrip in Figure 4A.

Movie S3: A timelapse FRAP-TIRF movie showing the dynamics of the unbound Fat4 on the basal membrane of the Fat4 expressing cell. Movie used to generate filmstrip in Figure 4C.

Github repository - All analysis code can be found at [49]

Figure 2 – source data 1: A source data used to produce Figure 2, Figure 2 – figure supplement 1 and Figure 2 – figure supplement 2. The excel file contain two tabs corresponding to the two experimental sets. The rows include: IDs_xh are the Ds values for every cell in a batch, IFat_xh are the Fat values for every cell in a batch, IFatDsAccumulating_xh are the Fat and Ds values of cell that have accumulation boundaries, and IFatDsNonAccumulating_xh are Fat and Ds values for cells that share a Fat-Ds interface without accumulation.

References

1 Adler, P. N. Planar signaling and morphogenesis in Drosophila. *Dev Cell* **2**, 525-535, (2002).

2 Lewis, J. & Davies, A. Planar cell polarity in the inner ear: how do hair cells acquire their oriented structure? *J Neurobiol* **53**, 190-201, (2002).

3 Lawrence, P. A., Struhl, G. & Casal, J. Planar cell polarity: one or two pathways? *Nat Rev Genet* **8**, 555-563, (2007).

4 Wang, Y. & Nathans, J. Tissue/planar cell polarity in vertebrates: new insights and new questions. *Development* **134**, 647-658, (2007).

5 Goodrich, L. V. & Strutt, D. Principles of planar polarity in animal development. *Development* **138**, 1877-1892, (2011).

6 Strutt, H. & Strutt, D. Asymmetric localisation of planar polarity proteins: Mechanisms and consequences. *Semin Cell Dev Biol* **20**, 957-963, (2009).

7 Montcouquiol, M. *et al.* Identification of Vangl2 and Scrb1 as planar polarity genes in mammals. *Nature* **423**, 173-177, (2003).

8 Dabdoub, A. & Kelley, M. W. Planar cell polarity and a potential role for a Wnt morphogen gradient in stereociliary bundle orientation in the mammalian inner ear. *J Neurobiol* **64**, 446-457, (2005).

9 Saburi, S. *et al.* Loss of Fat4 disrupts PCP signaling and oriented cell division and leads to cystic kidney disease. *Nat Genet* **40**, 1010-1015, (2008).

10 Singh, J. & Mlodzik, M. Planar cell polarity signaling: coordination of cellular orientation across tissues. *Wiley Interdiscip Rev Dev Biol* **1**, 479-499, (2012).

11 Sharma, P. & McNeill, H. Fat and Dachsous cadherins. *Prog Mol Biol Transl Sci* **116**, 215-235, (2013).

12 Matakatsu, H. & Blair, S. S. Interactions between Fat and Dachsous and the regulation of planar cell polarity in the Drosophila wing. *Development* **131**, 3785-3794, (2004).

13 Matis, M. & Axelrod, J. D. Regulation of PCP by the Fat signaling pathway. *Genes Dev* **27**, 2207-2220, (2013).

14 Rock, R., Schrauth, S. & Gessler, M. Expression of mouse dchs1, fjx1, and fat-j suggests conservation of the planar cell polarity pathway identified in Drosophila. *Dev Dyn* **234**, 747-755, (2005).

15 Ishiuchi, T., Misaki, K., Yonemura, S., Takeichi, M. & Tanoue, T. Mammalian Fat and Dachsous cadherins regulate apical membrane organization in the embryonic cerebral cortex. *J Cell Biol* **185**, 959-967, (2009).

16 Katoh, M. Function and cancer genomics of FAT family genes (review). *Int J Oncol* **41**, 1913-1918, (2012).

17 Cappello, S. *et al.* Mutations in genes encoding the cadherin receptor-ligand pair DCHS1 and FAT4 disrupt cerebral cortical development. *Nat Genet* **45**, 1300-1308, (2013).

18 Casal, J., Lawrence, P. A. & Struhl, G. Two separate molecular systems, Dachsous/Fat and Starry night/Frizzled, act independently to confer planar cell polarity. *Development* **133**, 4561-4572, (2006).

19 Lawrence, P. A., Struhl, G. & Casal, J. Do the protocadherins Fat and Dachsous link up to determine both planar cell polarity and the dimensions of organs? *Nat Cell Biol* **10**, 1379-1382, (2008).

20 Strutt, D. Gradients and the specification of planar polarity in the insect cuticle. *Cold Spring Harb Perspect Biol* **1**, a000489, (2009).

21 Hale, R., Brittle, A. L., Fisher, K. H., Monk, N. A. & Strutt, D. Cellular interpretation of the long-range gradient of Four-jointed activity in the Drosophila wing. *Elife* **4**, (2015).

22 Abley, K. *et al.* An intracellular partitioning-based framework for tissue cell polarity in plants and animals. *Development* **140**, 2061-2074, (2013).

23 Axelrod, J. D. & Tomlin, C. J. Modeling the control of planar cell polarity. *Wiley Interdiscip Rev Syst Biol Med* **3**, 588-605, (2011).

24 Amonlirdviman, K. *et al.* Mathematical modeling of planar cell polarity to understand domineering nonautonomy. *Science* **307**, 423-426, (2005).

25 Le Garrec, J. F., Lopez, P. & Kerszberg, M. Establishment and maintenance of planar epithelial cell polarity by asymmetric cadherin bridges: a computer model. *Dev Dyn* **235**, 235-246, (2006).

26 Fischer, S., Houston, P., Monk, N. A. & Owen, M. R. Is a persistent global bias necessary for the establishment of planar cell polarity? *PLoS One* **8**, e60064, (2013).

27 Mani, M., Goyal, S., Irvine, K. D. & Shraiman, B. I. Collective polarization model for gradient sensing via Dachsous-Fat intercellular signaling. *Proc Natl Acad Sci U S A* **110**, 20420-20425, (2013).

28 Burak, Y. & Shraiman, B. I. Order and stochastic dynamics in Drosophila planar cell polarity. *PLoS Comput Biol* **5**, e1000628, (2009).

29 Desai, R. A., Gao, L., Raghavan, S., Liu, W. F. & Chen, C. S. Cell polarity triggered by cell-cell adhesion via E-cadherin. *J Cell Sci* **122**, 905-911, (2009).

30 Chen, C. P., Posy, S., Ben-Shaul, A., Shapiro, L. & Honig, B. H. Specificity of cell-cell adhesion by classical cadherins: Critical role for low-affinity dimerization through beta-strand swapping. *Proc Natl Acad Sci U S A* **102**, 8531-8536, (2005).

31 Zhang, Y., Sivasankar, S., Nelson, W. J. & Chu, S. Resolving cadherin interactions and binding cooperativity at the single-molecule level. *Proc Natl Acad Sci U S A* **106**, 109-114, (2009).

32 Khait, I. *et al.* Quantitative analysis of Delta-like-1 membrane dynamics elucidates the role of contact geometry on Notch signaling. (2015).

33 de Beco, S., Gueudry, C., Amblard, F. & Coscoy, S. Endocytosis is required for E-cadherin redistribution at mature adherens junctions. *Proc Natl Acad Sci U S A* **106**, 7010-7015, (2009).

34 Brittle, A. L., Repiso, A., Casal, J., Lawrence, P. A. & Strutt, D. Four-jointed modulates growth and planar polarity by reducing the affinity of dachsous for fat. *Curr Biol* **20**, 803-810, (2010).

35 Leckband, D. & Prakasam, A. Mechanism and dynamics of cadherin adhesion. *Annu Rev Biomed Eng* **8**, 259-287, (2006).

36 Rogulja, D. & Irvine, K. D. Regulation of cell proliferation by a morphogen gradient. *Cell* **123**, 449-461, (2005).

37 Rogulja, D., Rauskolb, C. & Irvine, K. D. Morphogen control of wing growth through the Fat signaling pathway. *Dev Cell* **15**, 309-321, (2008).

38 Aigouy, B. *et al.* Cell flow reorients the axis of planar polarity in the wing epithelium of Drosophila. *Cell* **142**, 773-786, (2010).

39 Rovira, M., Saavedra, P., Casal, J. & Lawrence, P. A. Regions within a single epidermal cell of Drosophila can be planar polarised independently. *Elife* **4**, (2015).

40 Wu, Y. *et al.* Cooperativity between trans and cis interactions in cadherin-mediated junction formation. *Proc Natl Acad Sci U S A* **107**, 17592-17597, (2010).

41 Matis, M., Russler-Germain, D. A., Hu, Q., Tomlin, C. J. & Axelrod, J. D. Microtubules provide directional information for core PCP function. *Elife* **3**, e02893, (2014).

42 Tsukasaki, Y. *et al.* Giant cadherins Fat and Dachsous self-bend to organize properly spaced intercellular junctions. *Proc Natl Acad Sci U S A* **111**, 16011-16016, (2014).

43 Saavedra, P., Vincent, J. P., Palacios, I. M., Lawrence, P. A. & Casal, J. Plasticity of both planar cell polarity and cell identity during the development of Drosophila. *Elife* **3**, e01569, (2014).

44 Gibson, D. G. *et al.* Enzymatic assembly of DNA molecules up to several hundred kilobases. *Nat Methods* **6**, 343-345, (2009).
45 Nelson, C. M., Liu, W. F. & Chen, C. S. Manipulation of cell-cell adhesion using bowtie-shaped microwells. *Methods Mol Biol* **370**, 1-10, (2007).
46 Sommer, C., Straehle, C., Kothe, U. & Hamprecht, F. A. Ilastik: Interactive Learning and Segmentation Toolkit. *I S Biomed Imaging*, 230-233, (2011).
47 Smith, M. B. *et al.* Segmentation and tracking of cytoskeletal filaments using open active contours. *Cytoskeleton (Hoboken)* **67**, 693-705, (2010).
48 Goehring, N. W., Chowdhury, D., Hyman, A. A. & Grill, S. W. FRAP analysis of membrane-associated proteins: lateral diffusion and membrane-cytoplasmic exchange. *Biophys J* **99**, 2443-2452, (2010).
49 Loza, O. *et al.* Fat_Ds_Analysis 8566587b. *Github* **https://github.com/idse/FatDs/**, (2017).

Figure 1

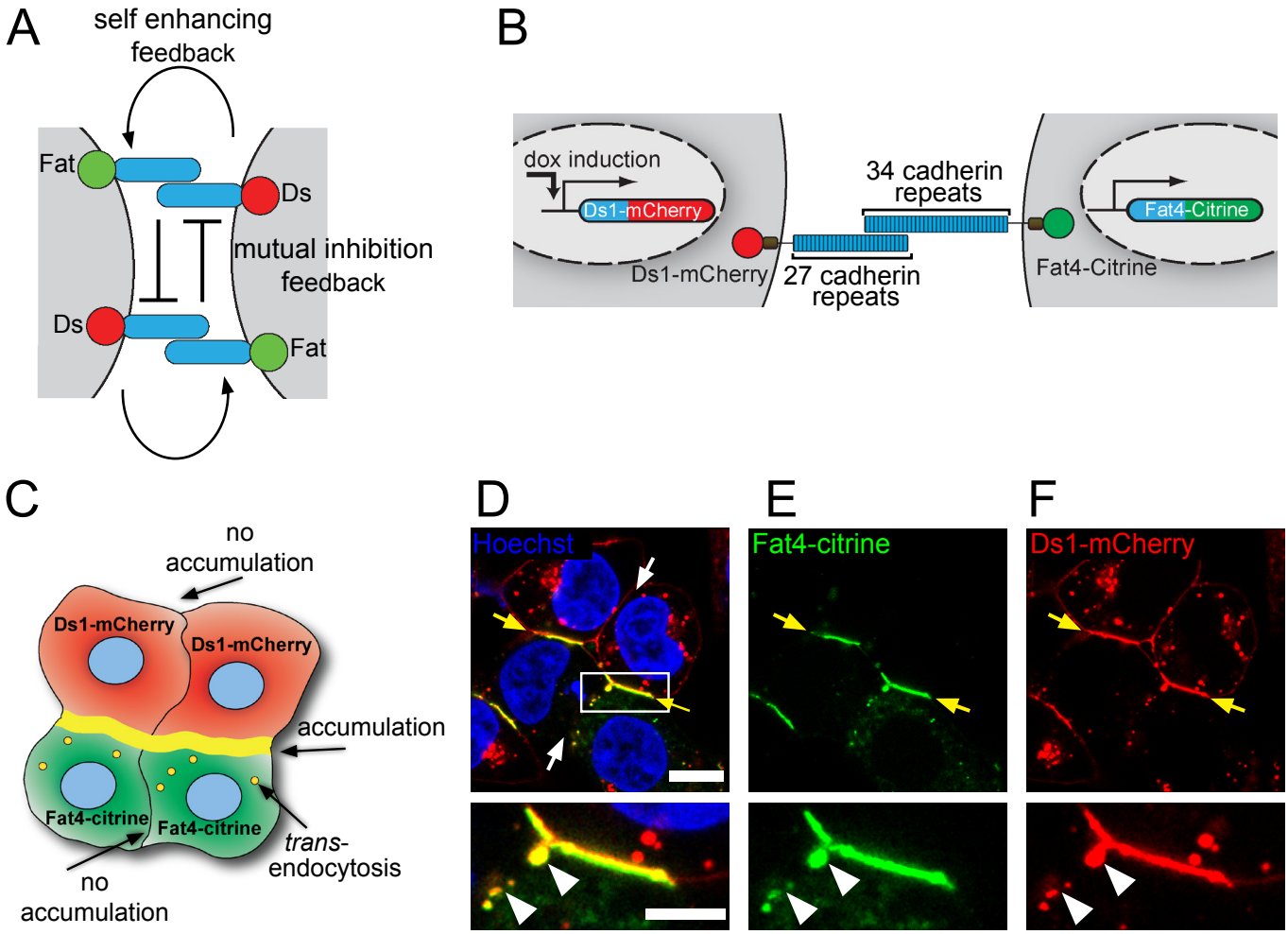
A
self enhancing feedback
Fat
Ds
mutual inhibition feedback
Ds
Fat
B
dox induction
Ds1-mCherry
34 cadherin repeats
Fat4-Citrine
Ds1-mCherry
27 cadherin repeats
Fat4-Citrine
C
no accumulation
Ds1-mCherry
Ds1-mCherry
accumulation
Fat4-citrine
Fat4-citrine
trans-endocytosis
no accumulation
D
Hoechst
E
Fat4-citrine
F
Ds1-mCherry

Figure 1- figure supplement 1

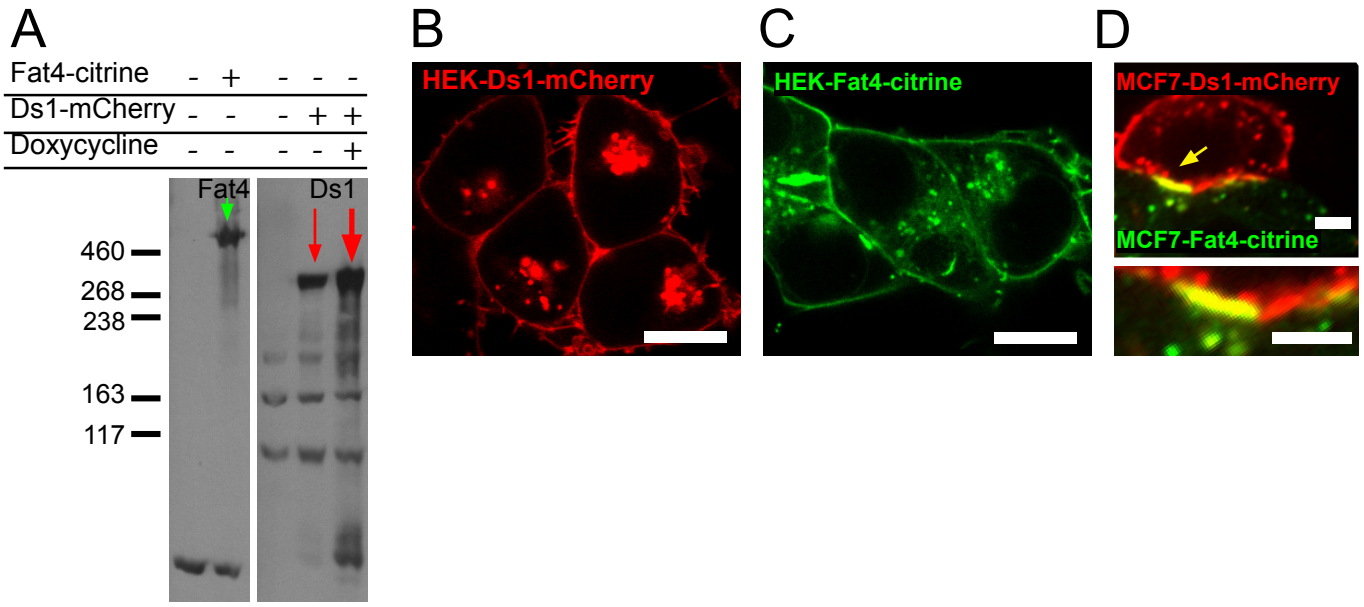

Figure 2

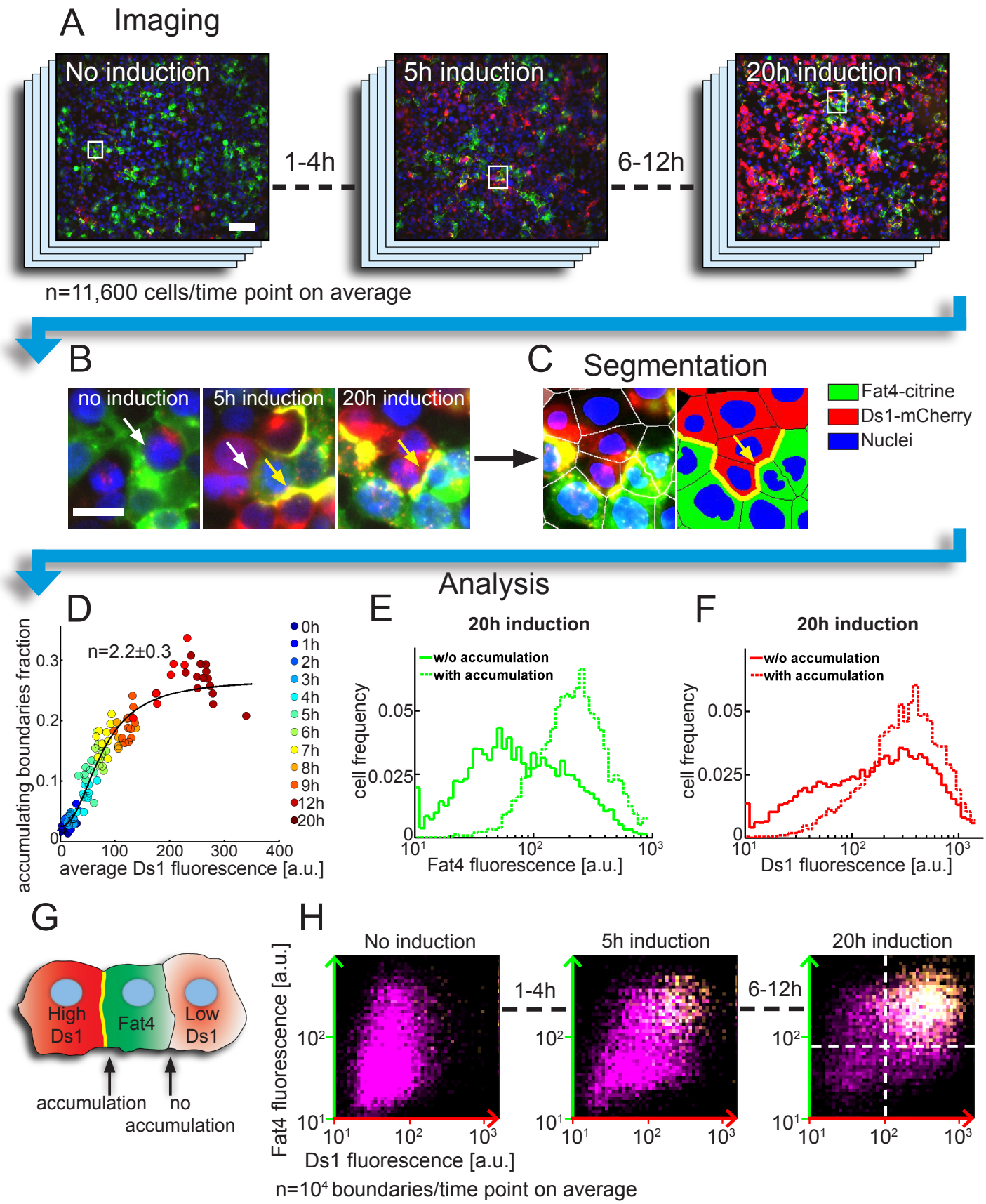
A Imaging
No induction
5h induction
20h induction
1-4h
6-12h
n=11,600 cells/time point on average
B
no induction
5h induction
20h induction
C Segmentation
Fat4-citrine
Ds1-mCherry
Nuclei
Analysis
D
n=2.2±0.3
accumulating boundaries fraction
average Ds1 fluorescence [a.u.]
0h
1h
2h
3h
4h
5h
6h
7h
8h
9h
12h
20h
E
20h induction
w/o accumulation
with accumulation
cell frequency
Fat4 fluorescence [a.u.]
F
20h induction
w/o accumulation
with accumulation
cell frequency
Ds1 fluorescence [a.u.]
G
High Ds1
Fat4
Low Ds1
accumulation
no accumulation
H
No induction
5h induction
20h induction
1-4h
6-12h
Fat4 fluorescence [a.u.]
Ds1 fluorescence [a.u.]
n=10⁴ boundaries/time point on average

Figure 2 - figure supplement 1

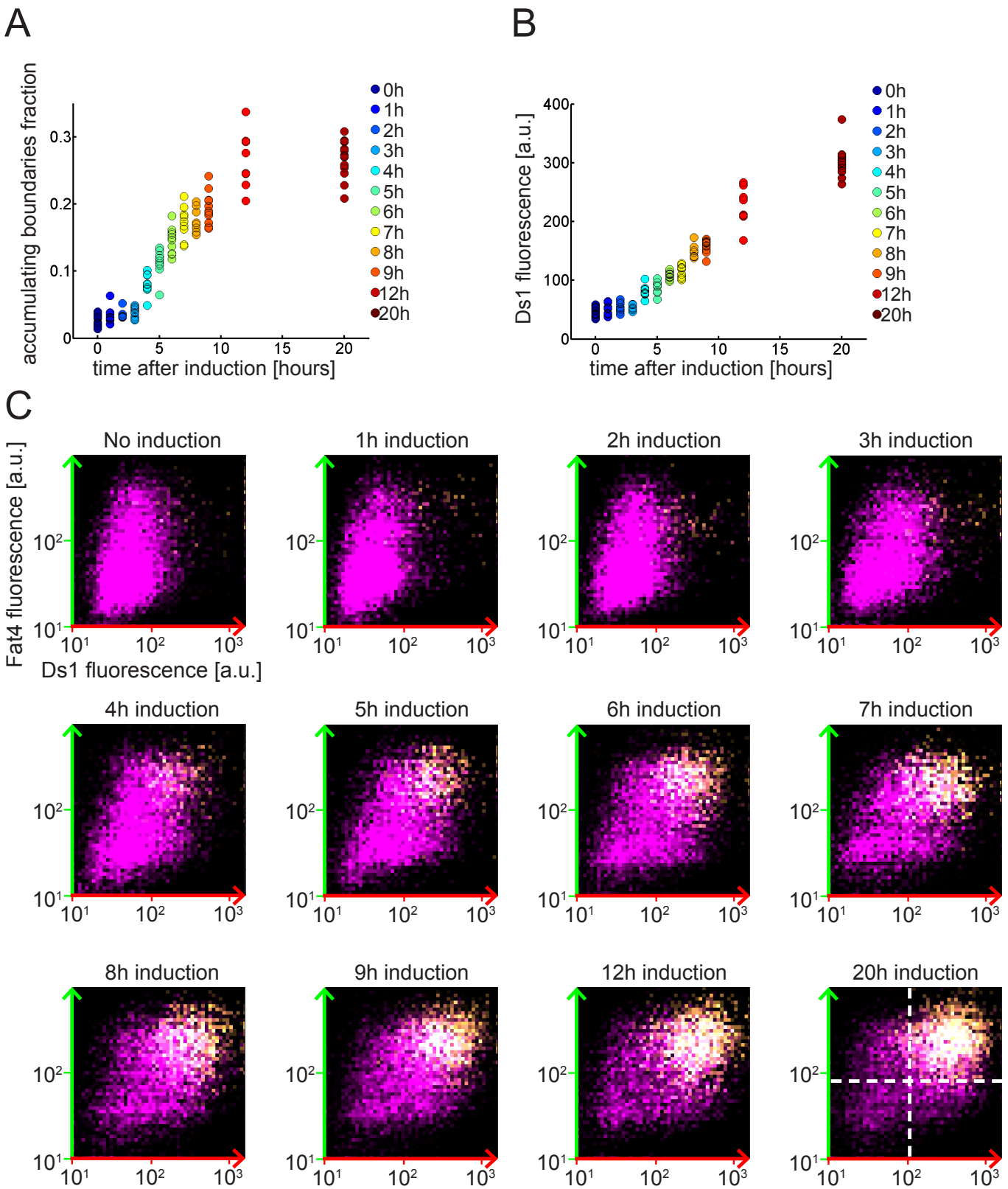

Figure 2 - figure supplement 2

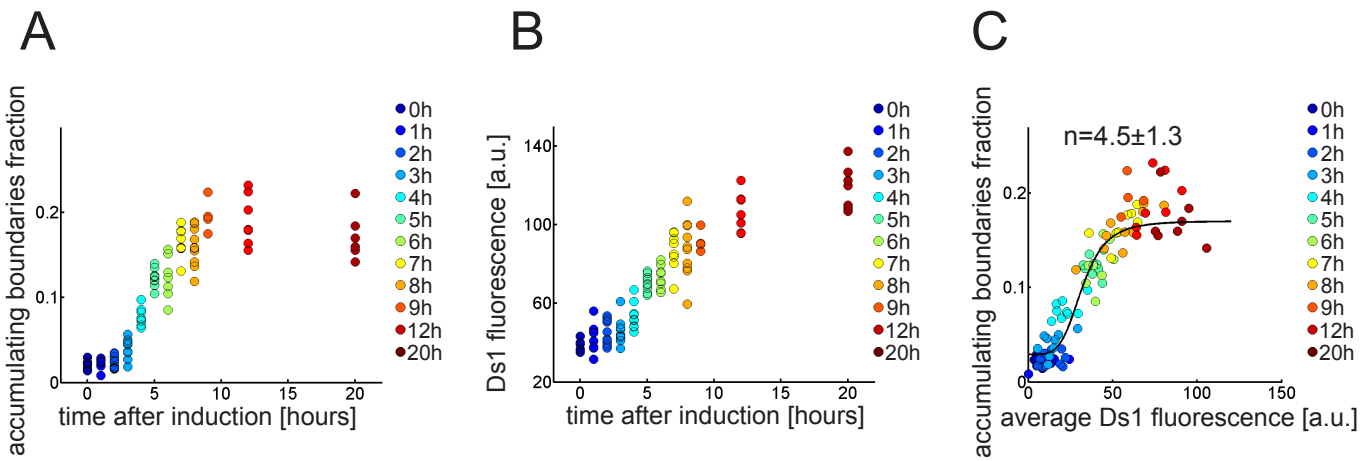

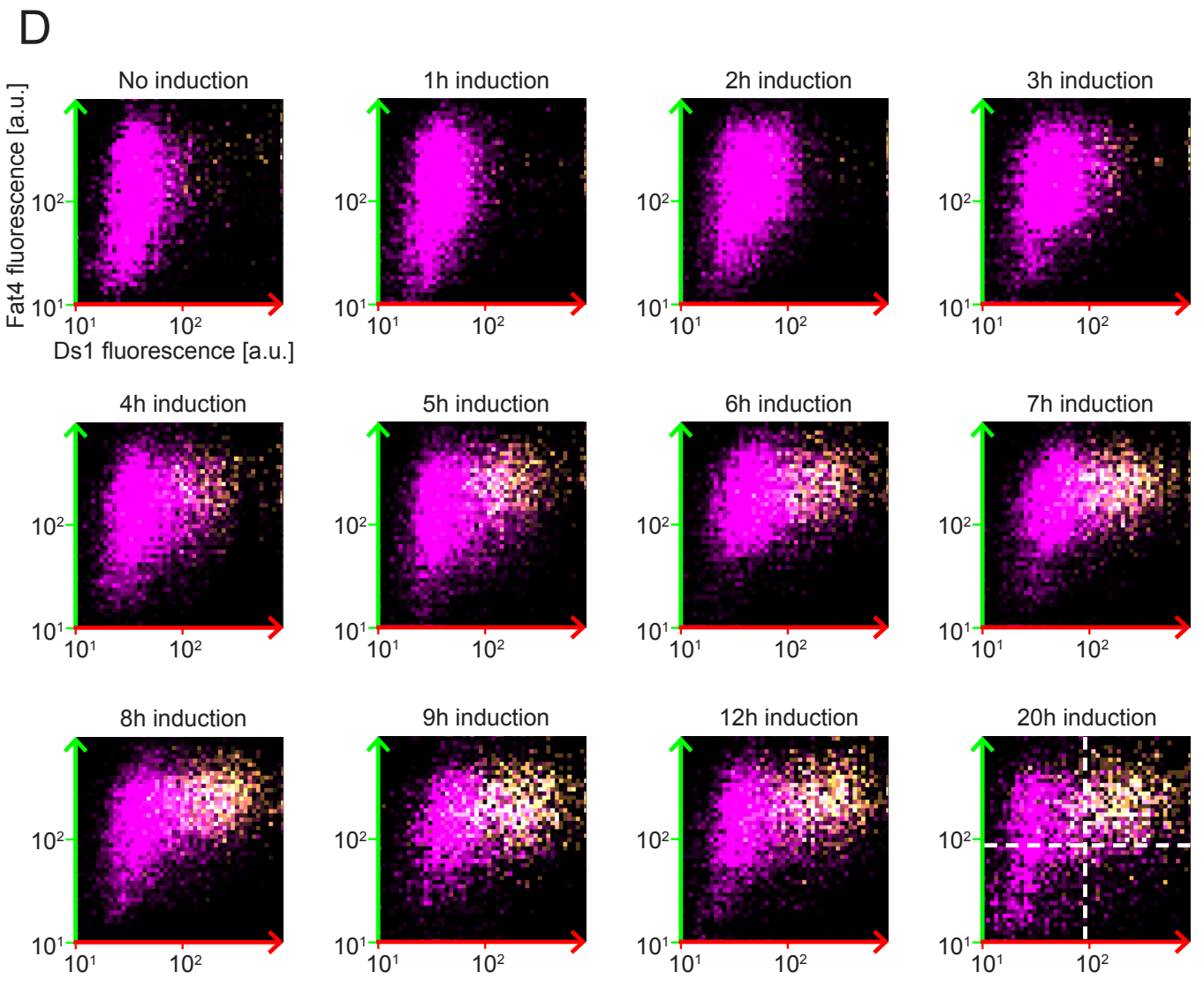

Figure 3

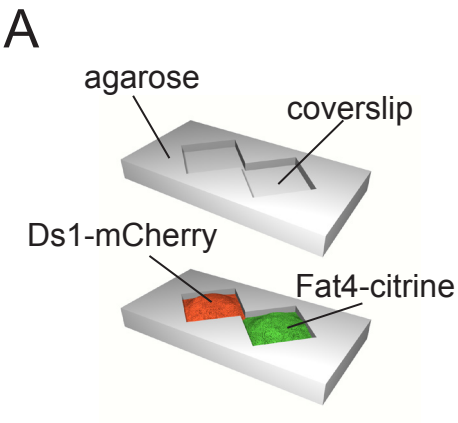
A
agarose
coverslip
Ds1-mCherry
Fat4-citrine

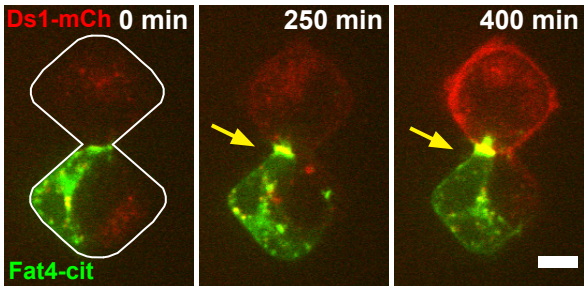
B
Ds1-mCh 0 min
250 min
400 min
Fat4-cit

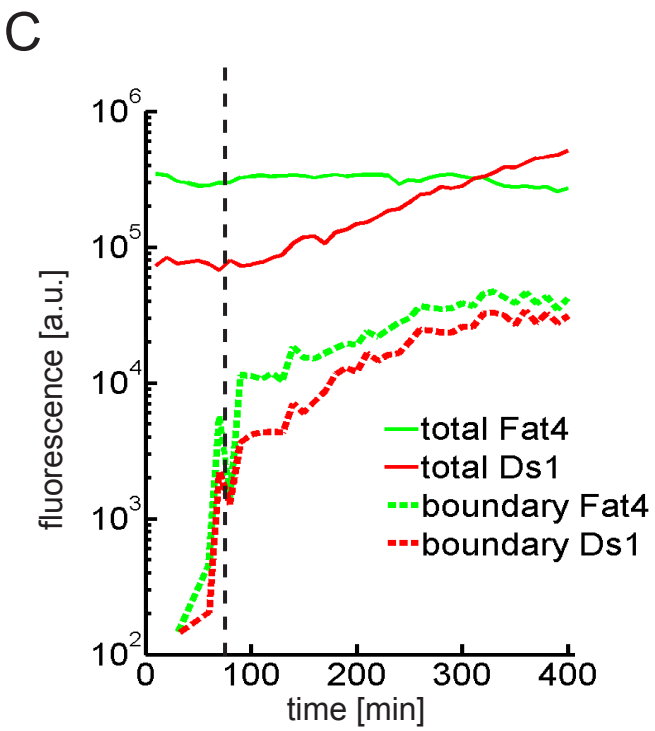
C
fluorescence [a.u.]
time [min]
total Fat4
total Ds1
boundary Fat4
boundary Ds1

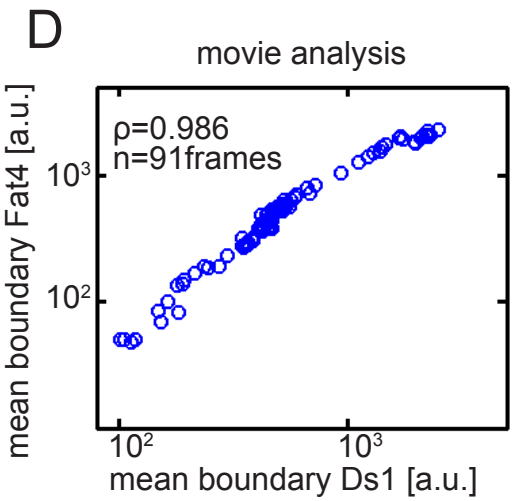
D
movie analysis
ρ=0.986
n=91frames
mean boundary Fat4 [a.u.]
mean boundary Ds1 [a.u.]

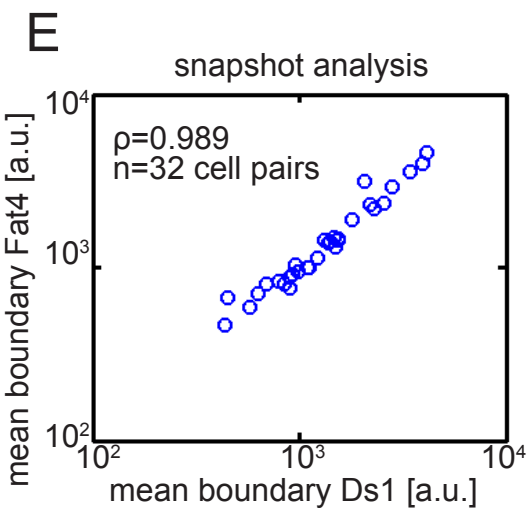
E
snapshot analysis
ρ=0.989
n=32 cell pairs
mean boundary Fat4 [a.u.]
mean boundary Ds1 [a.u.]

Figure 3 - figure supplement 1

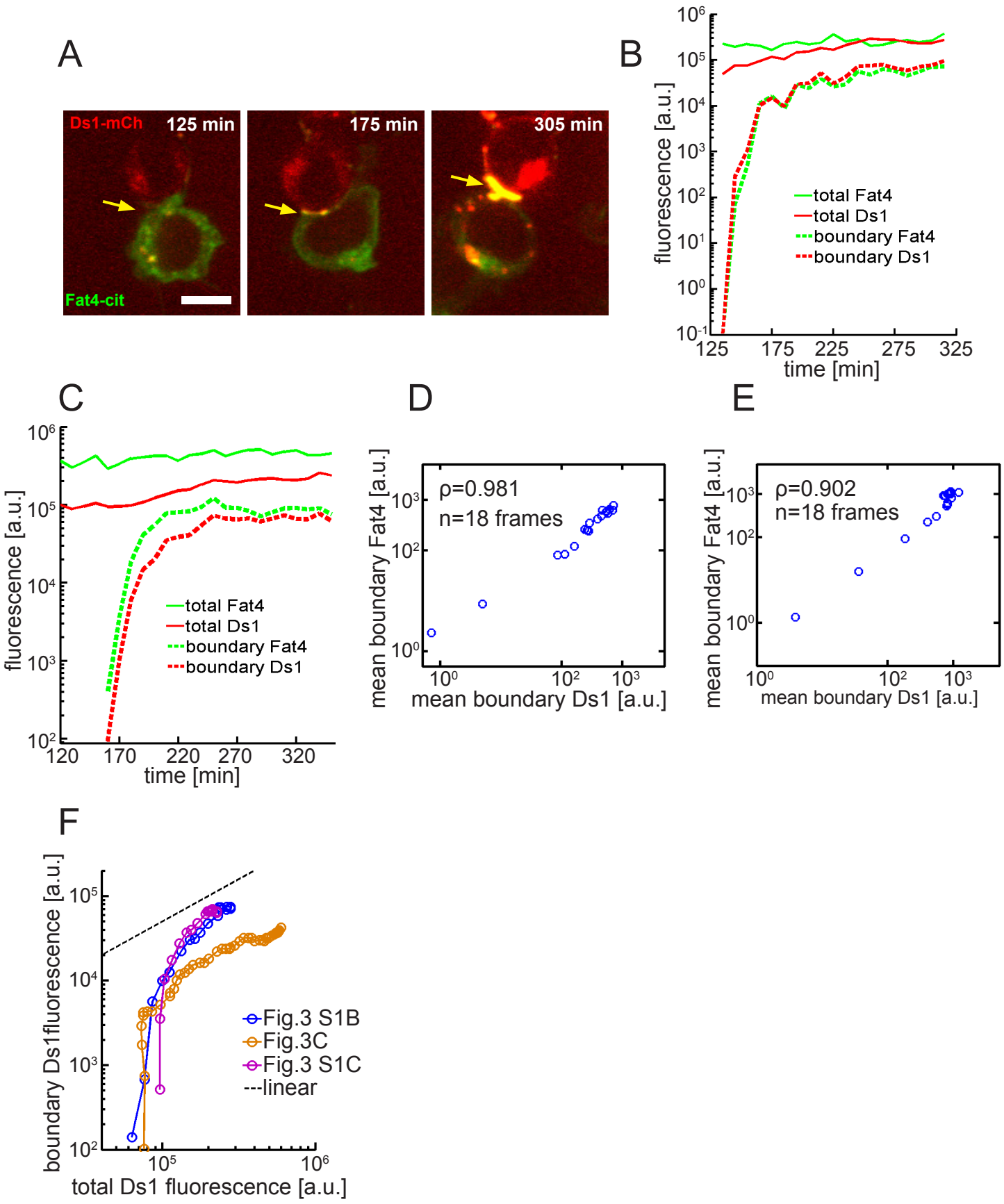

Figure 3 - figure supplement 2

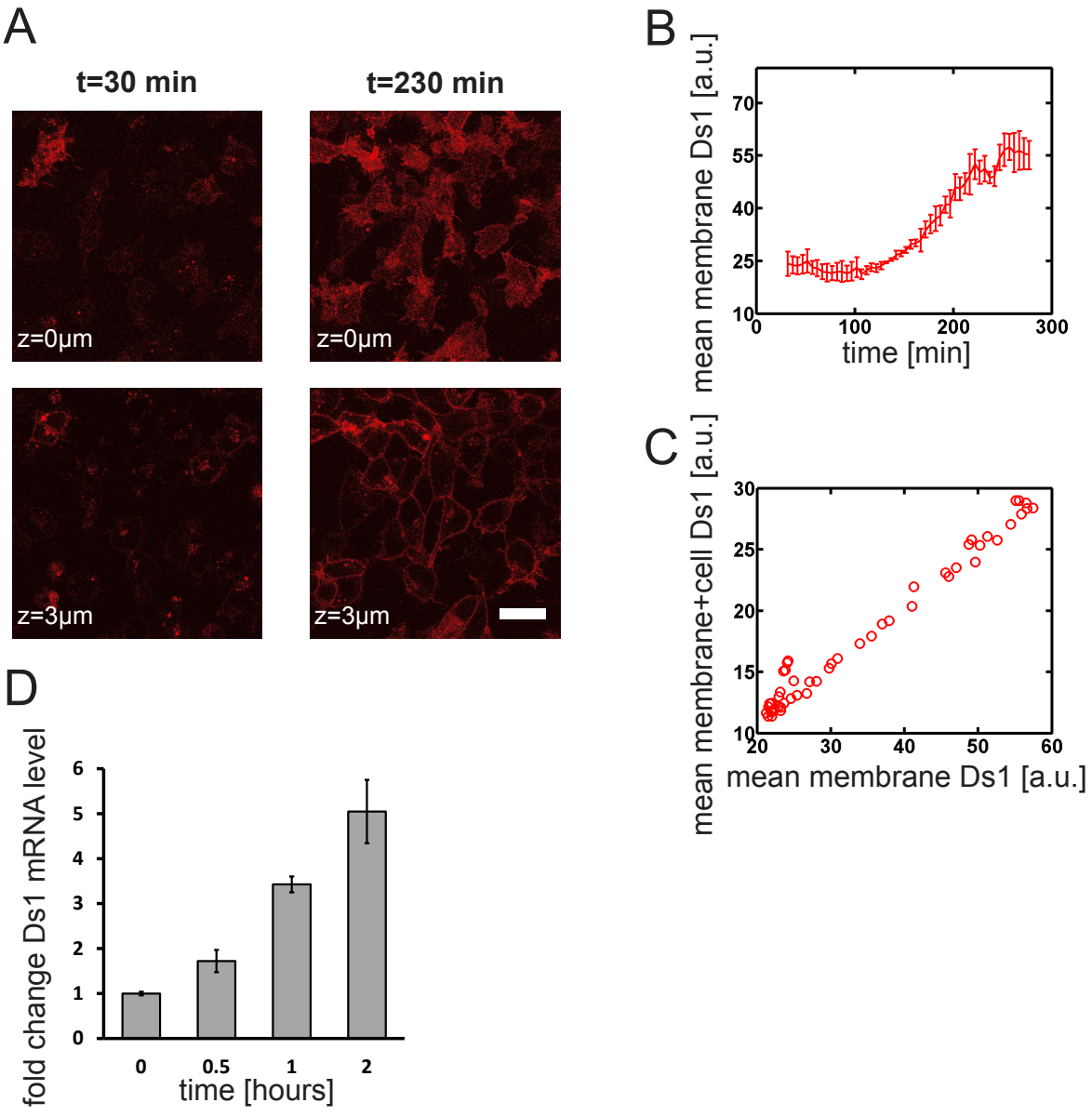

Figure 4

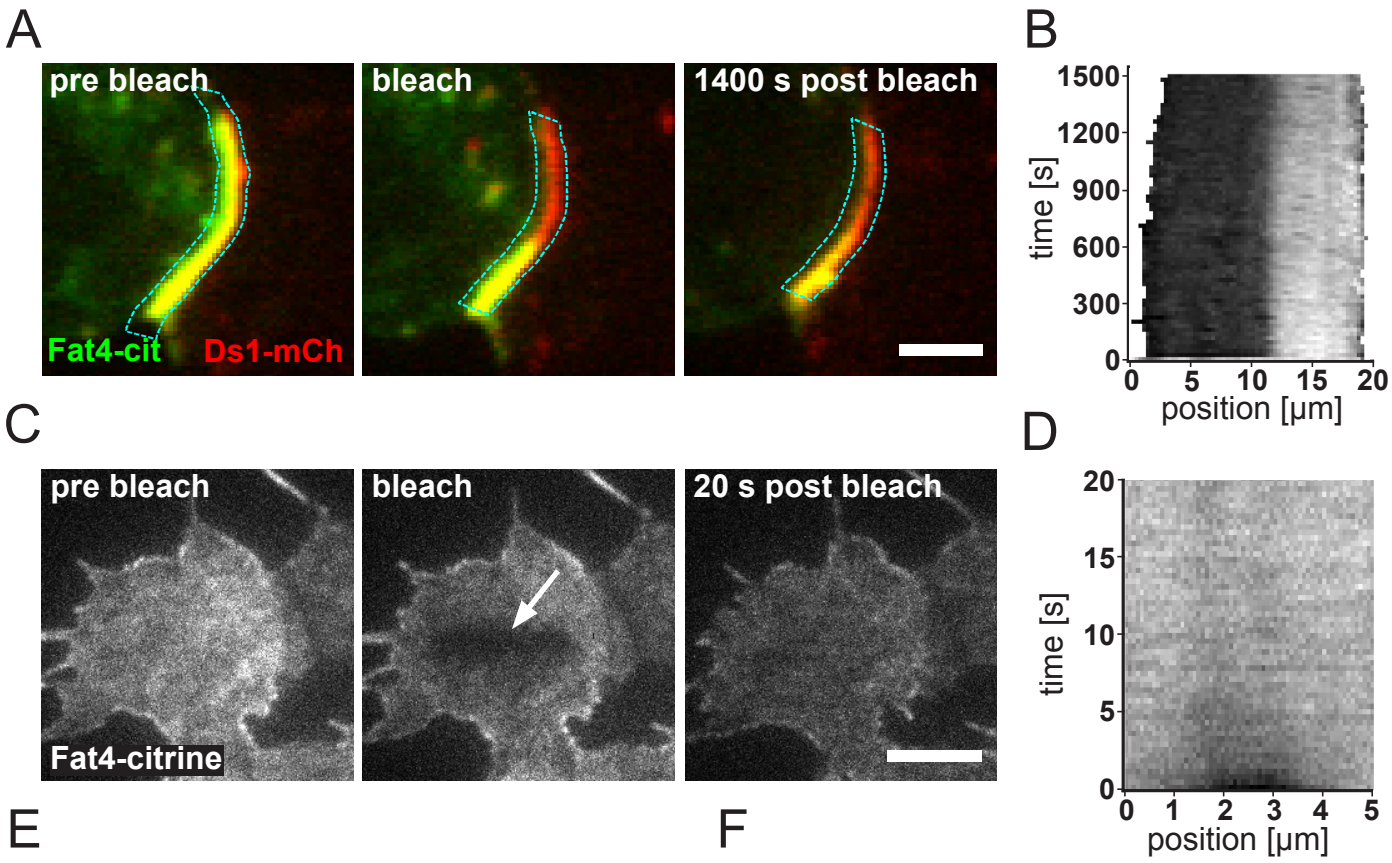
A
pre bleach
bleach
1400 s post bleach
Fat4-cit
Ds1-mCh
B
time [s]
position [μm]
C
pre bleach
bleach
20 s post bleach
Fat4-citrine
D
time [s]
position [μm]

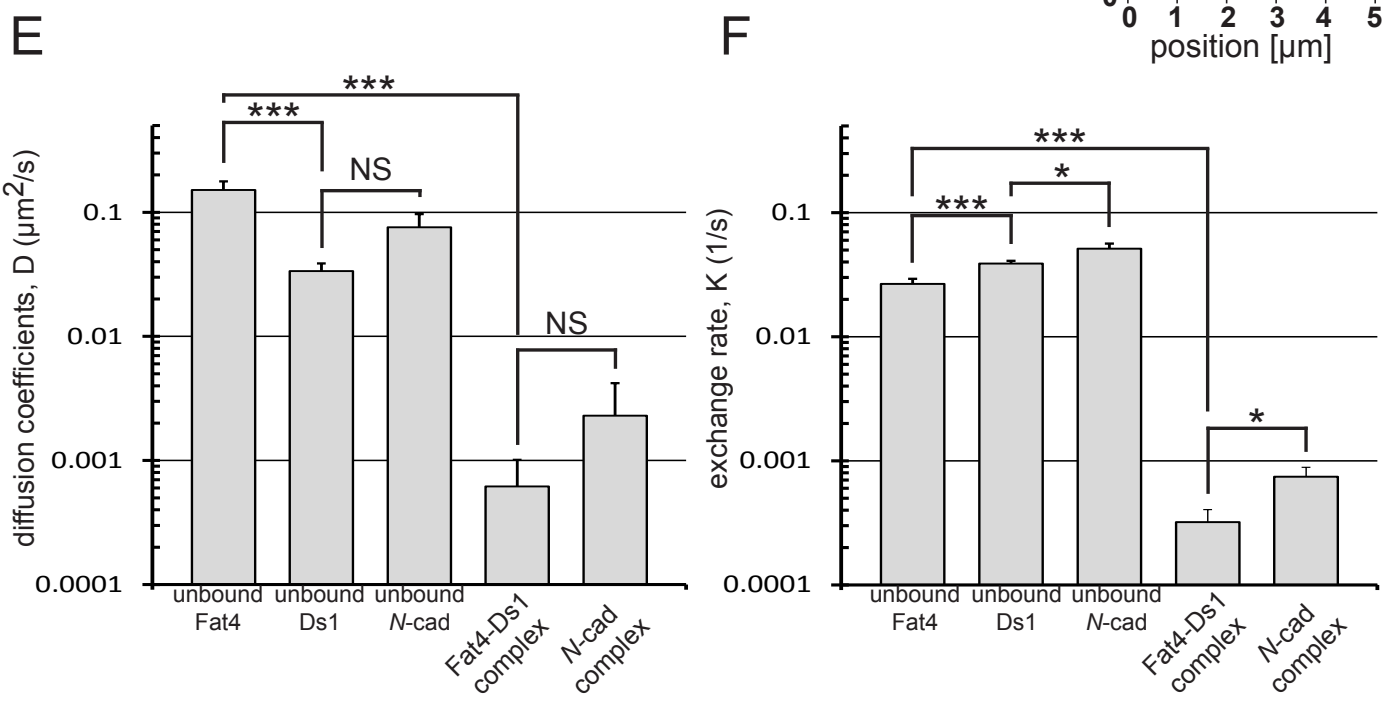
E
diffusion coefficients, D (μm²/s)
***
***
NS
NS
unbound Fat4
unbound Ds1
unbound N-cad
Fat4-Ds1 complex
N-cad complex
F
exchange rate, K (1/s)
***
*
***
*
unbound Fat4
unbound Ds1
unbound N-cad
Fat4-Ds1 complex
N-cad complex

Figure 4 - figure supplement 1

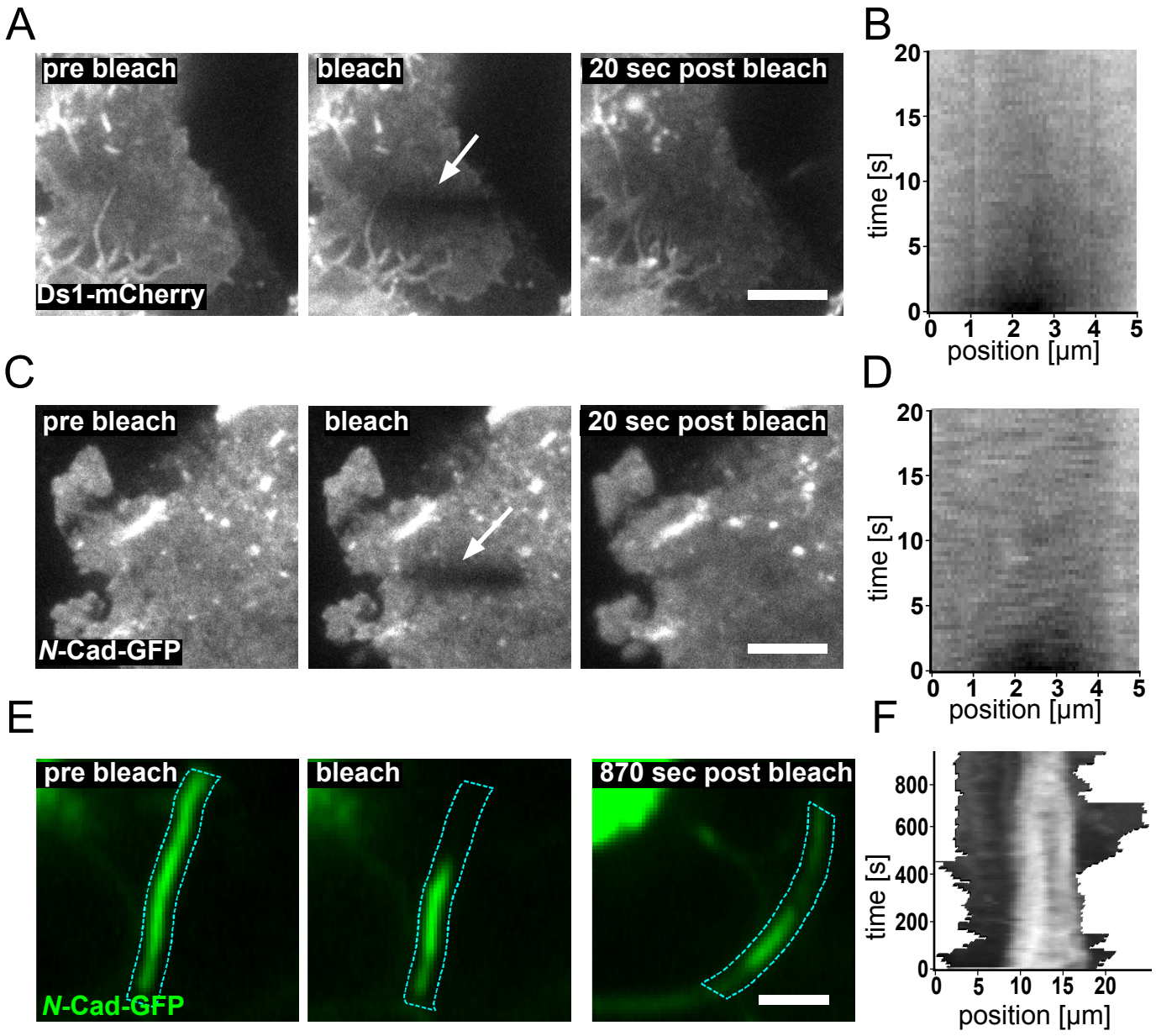

Figure 5

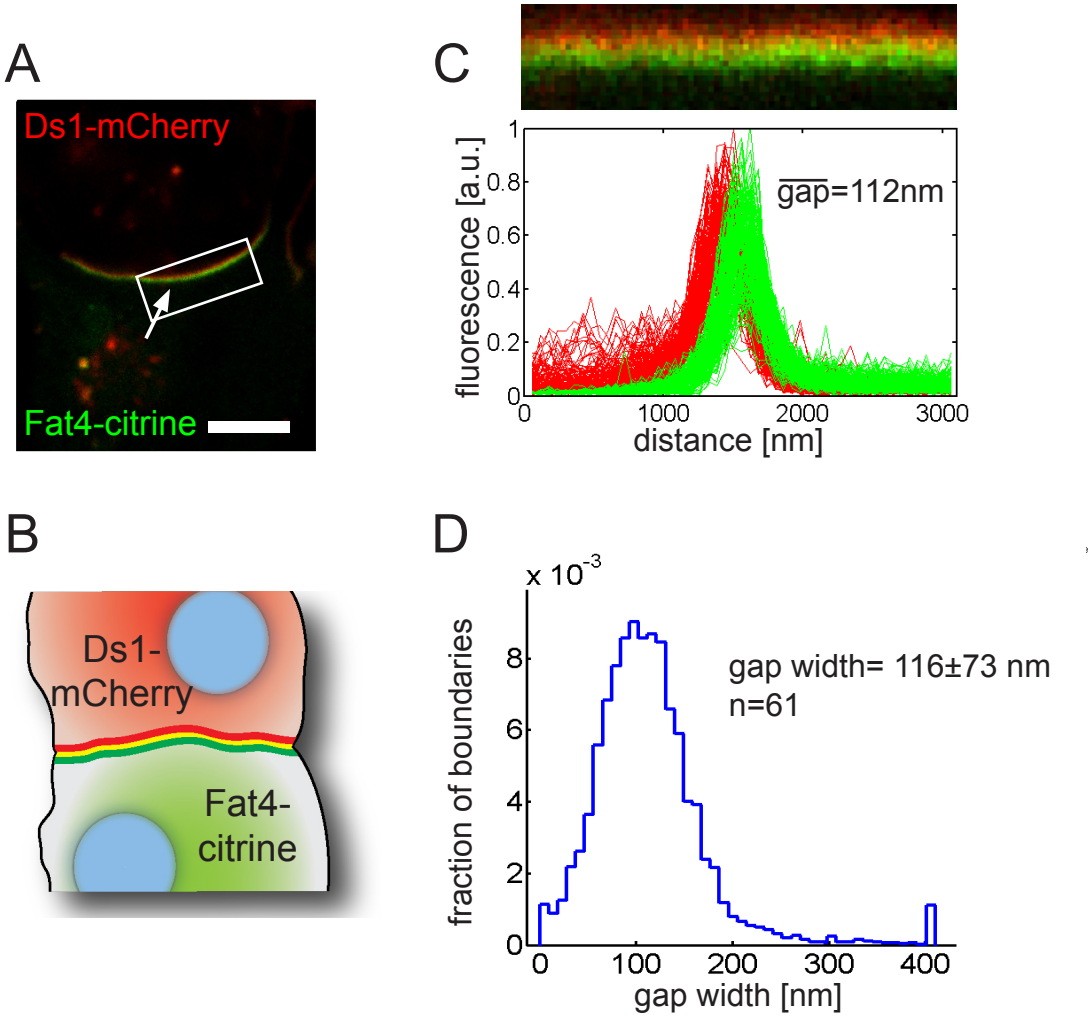
A
Ds1-mCherry
Fat4-citrine
C
fluorescence [a.u.]
gap=112nm
distance [nm]
B
Ds1-
mCherry
Fat4-
citrine
D
x 10-3
fraction of boundaries
gap width= 116±73 nm
n=61
gap width [nm]

Figure 5 - figure supplement 1

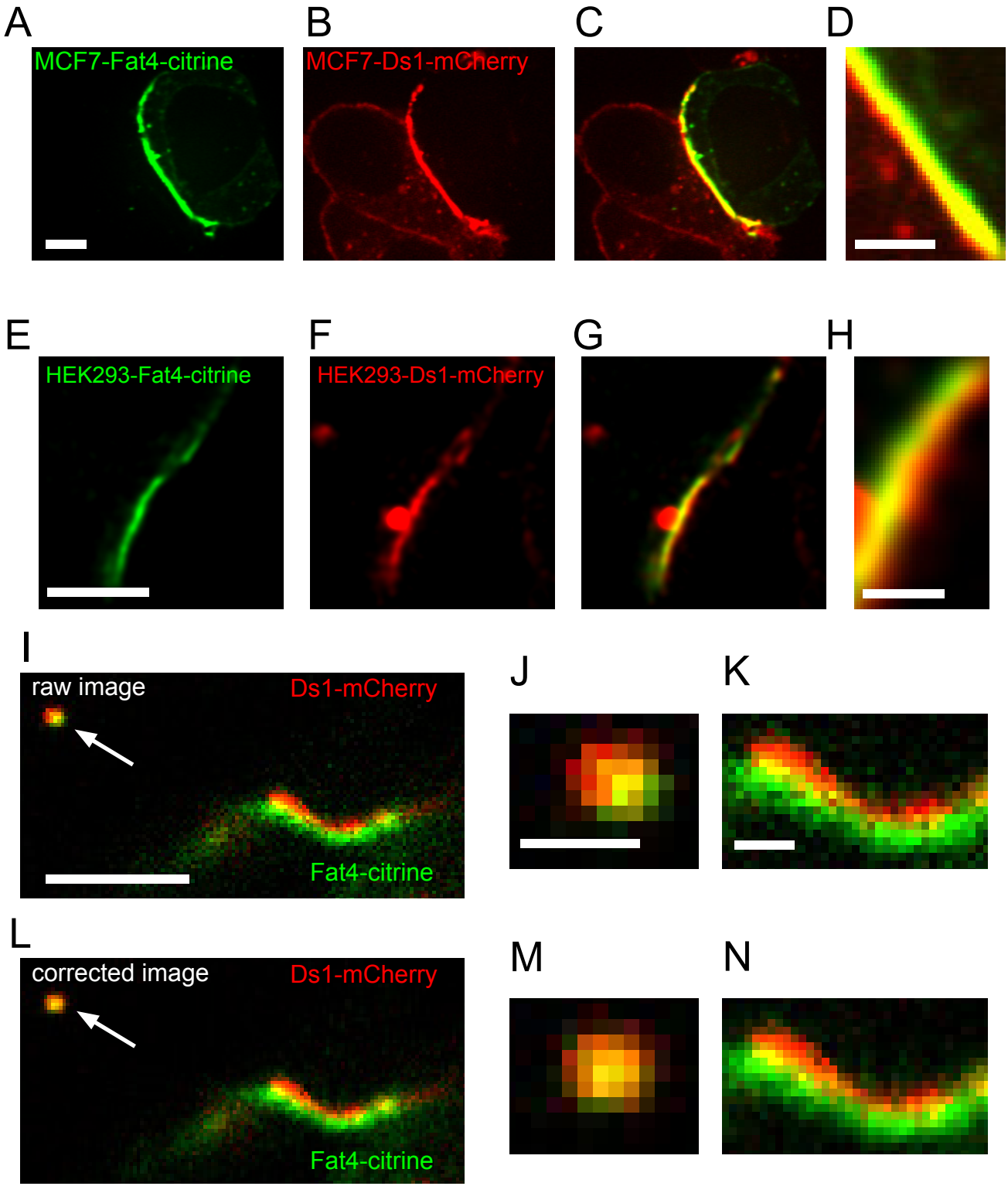

Figure 6

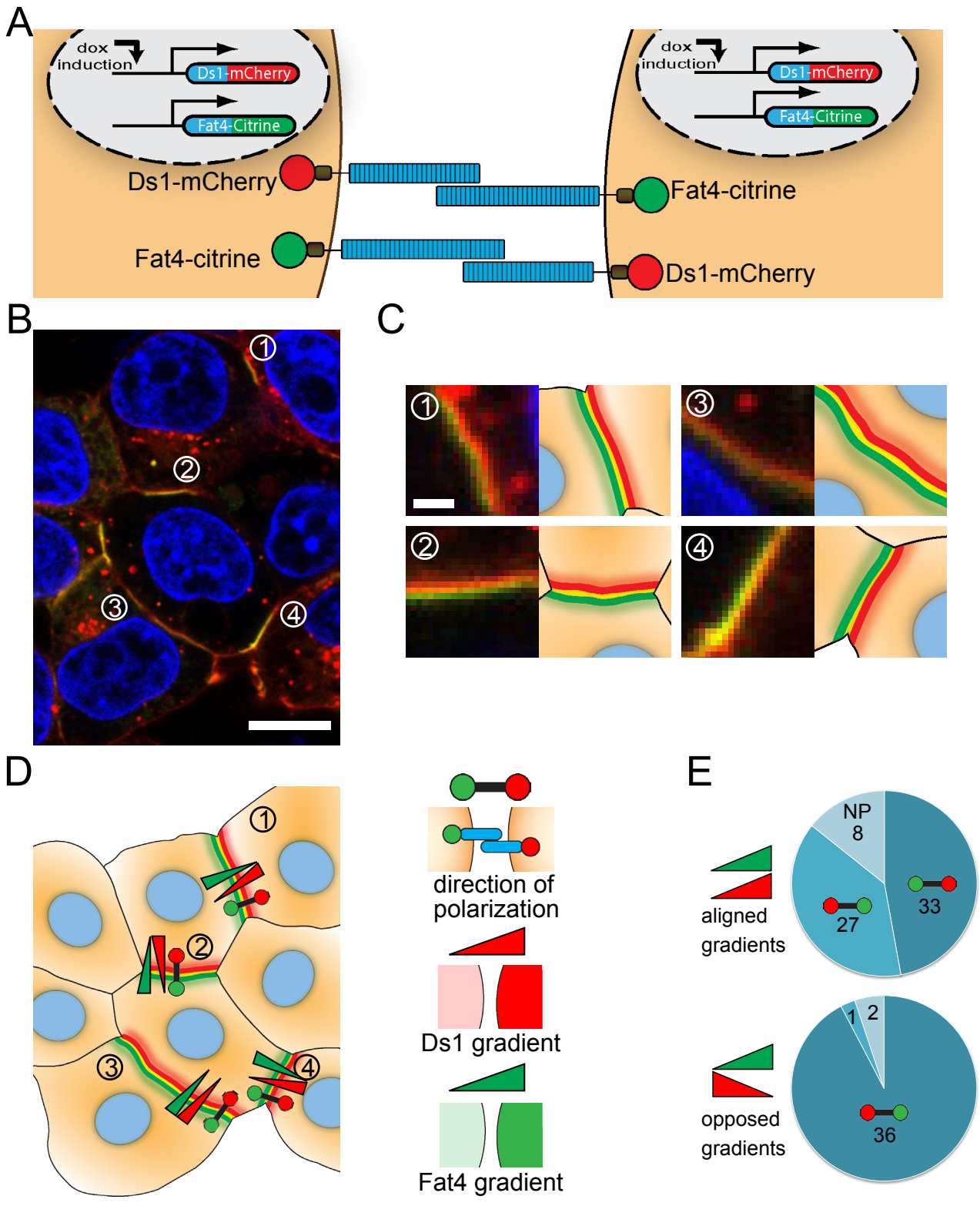
A
dox induction
Ds1-mCherry
Fat4-Citrine
Ds1-mCherry
Fat4-citrine
Fat4-citrine
Ds1-mCherry
B
C
D
direction of polarization
Ds1 gradient
Fat4 gradient
E
aligned gradients
NP 8
33
27
opposed gradients
1
2
36

Figure 6 - figure supplement 1